Journal of Geophysical Research: Space Physics

RESEARCH ARTICLE
10.1029/2017JA024701

Key Points:
- We present a case where ionospheric fast flows in the midnight sector main auroral oval subsided during a transpolar arc brightening
- We suggest that subsidence of these flows during the transpolar arc brightening is closely related to the extent of nightside reconnection
- The static nature of the arc is explained by its proximity to the cusp, where lobe reconnection signatures are observed by Cluster

Supporting Information:
- Supporting Information S1
- Figure S1
- Movie S1

Correspondence to:
M. Nowada and Q.-Q. Shi ,
moto.nowada@sdu.edu.cn;
sqq@sdu.edu.cn

Citation:
Nowada, M., Fear, R. C., Grocott, A., Shi, Q.-Q., Yang, J., Zong, Q.-G., et al. (2018). Subsidence of ionospheric flows triggered by magnetotail magnetic reconnection during transpolar arc brightening. *Journal of Geophysical Research: Space Physics*, *123*. https://doi.org/10.1029/2017JA024701

Received 21 AUG 2017
Accepted 6 APR 2018
Accepted article online 19 APR 2018

Subsidence of Ionospheric Flows Triggered by Magnetotail Magnetic Reconnection During Transpolar Arc Brightening

Motoharu Nowada[1], Robert C. Fear[2], Adrian Grocott[3], Quan-Qi Shi[1], Jun Yang[1], Qiu-Gang Zong[4], Yong Wei[5], Sui-Yan Fu[4], Zu-Yin Pu[4], Bagrat Mailyan[1], and Hui Zhang[6]

[1]Center for Space Weather Sciences, Institute of Space Sciences, School of Space Science and Physics, Shandong University at Weihai, Weihai, China, [2]Department of Physics and Astronomy, University of Southampton, Southampton, UK, [3]Space and Planetary Physics Group, Department of Physics, Lancaster University, Lancaster, UK, [4]Institute of Space Physics and Applied Technology, School of Earth and Space Sciences, Peking University, Beijing, China, [5]Key Laboratory of Earth and Planetary Physics, Institute of Geology and Geophysics, Chinese Academy of Sciences, Beijing, China, [6]Geophysical Institute, University of Alaska Fairbanks, Fairbanks, AK, USA

Abstract A transpolar arc (TPA), which extended from postmidnight to prenoon, was seen on 16 September 2001 in the Northern Hemisphere under northward interplanetary magnetic field (IMF)-B_z and weakly dawnward IMF-B_y conditions. Super Dual Auroral Radar Network detected significant westward plasma flows just equatorward of the poleward edge of the midnight sector auroral oval. These plasma flows were confined to closed field lines and are identified as the ionospheric plasma flow signature of tail reconnection during IMF northward nonsubstorm intervals (TRINNIs). These TRINNI flows persisted for 53 min from prior to the TPA appearance to the cessation of TPA growth. They are usually observed before (and during) intervals when TPAs are present, but in this case, subsided after the TPA was completely connected to the dayside. Additional slower flows across the open/closed polar cap boundary were seen at the TPA onset time in the same magnetic local time sector as the nightside end of the TPA. These ionospheric flows suggest that magnetotail reconnection significantly contributed to the TPA formation, as proposed by Milan et al. (2005, https://doi.org/10.1029/2004JA010835). We propose a possible scenario for an absence of the TRINNI flows during the TPA brightening by considering the relation between the extent of the magnetotail reconnection line mapped onto nightside auroral oval and the TPA width; TRINNI flows would subside when the extent of X-line is comparable to the TPA width. Therefore, our results suggest that the fate (absence or presence) of TRINNI flows on closed field lines during the TPA formation would be closely related with magnetotail reconnection extent.

Plain Language Summary Magnetotail magnetic reconnection is considered as one of the most possible mechanisms to form transpolar arc (TPA), frequently seen under the northward interplanetary magnetic field conditions. The closed flux tube formed by nightside reconnection is considered as a source of the TPA. When magnetotail reconnection occurred, reconnection-accelerated westward plasma flows can be observed on the midnight sector of the main auroral oval. These flows are identified as the ionospheric plasma flow signature of tail reconnection during interplanetary magnetic field northward nonsubstorm intervals (TRINNIs), which is an indispensable phenomenon to physically explain the growth and brightening of TPA based on nightside magnetic reconnection as proposed by Milan et al. (2005, https://doi.org/10.1029/2004JA010835). We find the case where the ionospheric TRINNI flows were seen just before and during the TPA growth from the nightside main auroral oval, but subsided during the TPA brightening, when the TPA completely connected to the dayside region. There was clear evidence where magnetotail reconnection had persisted even during the TPA brightening in our case. In this study, based on the ionospheric plasma flow patterns just before and during the TPA formation, we discuss plausible cause why the ionospheric TRINNI flows subsided during the TPA brightening; nevertheless, magnetotail reconnection process persisted.

1. Introduction

The aurora with the shape of the Greek letter "θ," so-called "theta aurora," is one of many unsolved and mysterious auroral signatures that we do not completely understand. Its formation mechanism and physical

features have been investigated and discussed since the first image of a theta aurora was captured with an imager onboard DE-1 (Frank et al., 1982). Many researchers have focused on and debated the physical characteristics and formation mechanism of the "crossbar"-type emissive part of theta aurora within the polar cap, which is extended from the poleward edges of the nightside auroral oval toward the dayside region, identified as a "transpolar arc" (TPA).

When TPA formation mechanisms are discussed, the relationship between the orientation of the interplanetary magnetic field (IMF) and the occurrence and morphology of the TPA is frequently investigated. Based on a series of previous studies on the TPA's fundamental features (Gussenhoven, 1982; Kullen et al., 2002; Valladares et al., 1994, and references therein), the TPA occurrence is dominant when the IMF-B_z component is northward, with the location of its appearance and subsequent motion being governed by the orientation of the IMF-B_y component. The importance of the IMF-B_y component in the determination of the TPA location was confirmed by revealing the TPA signatures under changeable IMF-B_y and dominant IMF-B_z conditions (Cumnock, 2005; Cumnock et al., 1997, 2002). In particular, rapid IMF-B_y changes within about 20 min do not significantly impinge on the TPA location and motion (Cumnock, 2005; Cumnock et al., 2002). Kullen et al. (2002) suggested that not all cases of theta aurora follow this IMF-B_y control; however, Fear and Milan (2012a) showed that the IMF-B_y control is stronger if the IMF is lagged by a small number of hours (3–4 hr) or about 1–2 hr (Kullen et al., 2015). Auroral imager and ionospheric observations of TPAs revealed that a TPA is projected to the nightside plasma sheet or plasma sheet boundary layer and has similar particle features to the main oval of theta aurora (e.g., Chang et al., 1998; Cumnock, 2005; Cumnock et al., 1997, 2002; Frank et al., 1986; Kullen et al., 2002, and references therein), suggesting further that TPA is on closed field lines (e.g., Peterson & Shelley, 1984) and its formation process is attributed to the magnetotail phenomena (e.g., Kullen, 2000; Kullen & Janhunen, 2004; Milan et al., 2005).

Milan et al. (2005) addressed the issue of TPA formation based on the field line topology and the motion of flux tubes within the context of magnetospheric convection. They suggest that the TPA is formed by magnetic reconnection in a twisted magnetotail, occurring during northward IMF conditions, in which the footprints of the TPA-associated newly closed flux tubes straddle midnight and so are unable to form a return flow channel via either dawn or dusk. Instead, the flux gets "stuck" somewhere in the midnight sector and begins to grow as a protrusion into the polar cap. Further evidence for this model is provided by the above-mentioned time delay in the correlation between the IMF-B_y component and the location at which TPAs are observed (Fear & Milan, 2012a), as well as by a statistical link between TPAs and the ionospheric signatures of reconnection that were present in the Milan et al. (2005) case study and the statistical study of Fear and Milan (2012b).

Several other TPA formation models, constructed based on the relationship between the IMF orientation and associated magnetospheric field line topological changes, have been proposed. For example, recently, it is reported that the TPA might be formed by multiple solar wind plasma entries due to high-latitude lobe magnetic reconnection (Mailyan et al., 2015). On other details of the TPA formation, readers may refer to the reviews on the TPA formation by Zhu et al. (1997) and Fear and Milan (2012a).

Even though numerous models for TPA formation have been proposed, there have only been a small number of in situ observational results that have been able to test these models. Fear et al. (2014) showed observational evidence to support the magnetotail reconnection scenario of TPA formation. They observed two reversals in the direction of TPA motion (from dawnward to duskward then dawnward again) in the Southern Hemisphere, which corresponded to the expected variation in the size of lobe convection cells arising from changing IMF-B_y magnitudes and direction. The pitch angle distribution in the magnetotail associated with the TPA (see Figure 3 in Fear et al., 2014) shows high-energy electrons that were initially bidirectional (parallel and antiparallel to the field line) and then perpendicular to the field line. They claimed that this pitch angle profile is the same as the plasma sheet boundary layer, where the bidirectional components are dominant, and central plasma sheet with dominant perpendicular electrons. These observations are a signature that is supportive of the TPA forming an extended plasma sheet or plasma sheet boundary layer which protrudes into the magnetotail lobe. Furthermore, at the particular point where the perpendicular electrons were dominant, the intensity of the electron fluxes perpendicular to the field line was approximately double that of the fluxes in the field-aligned directions. They attributed the presence of closed magnetic flux to the mechanism put forward by Milan et al. (2005), where nightside magnetic

reconnection formed closed flux tubes and confined the accelerated electrons (due to the reconnection process and contraction of the closed field lines) within them in a similar manner to the formation of the regular plasma sheet at lower latitudes.

In this paper, we discuss ionospheric flow patterns associated with the formation of the TPA that was observed on 16 September 2001 based on both satellite and ground-based observations. Before the TPA appearance and during the growth of TPA, weak or clear westward fast ionospheric flows were seen on closed field lines (i.e., just equatorward of the poleward edge of the midnight sector main auroral oval). The TPA started to appear dimly from nightside and clearly extended to the dayside region just after the "return flows" were observed across the open/closed polar cap boundary. Hereafter, we identify a state where the TPA completely connected to the dayside region as "TPA brightening." The lifetime of the TPA was about 1 hr. The ionospheric flows on closed field lines and return flows are strongly supportive of the TPA formation model based on magnetotail magnetic reconnection that was proposed by Milan et al. (2005). The formation process of this TPA can be explained within the frame of the nightside reconnection model, although this TPA also grew as aligned to the dawnside main auroral oval. In a series of previous TPA studies (e.g., Fear & Milan, 2012b; Milan et al., 2005), the ionospheric flows on the closed field lines, indicating significant contribution of nightside reconnection to the TPA formation, persisted before and during the TPA appearance. However, in contrast to these previous studies, we show a case where ionospheric flows associated with nightside reconnection were observed just before the appearance and during the growth of the TPA, but this observation also shows a subsidence of flows once the TPA connected to the dayside auroral oval. The magnetic reconnection signature persists throughout the TPA's lifetime. We investigate the relationship between nightside magnetic reconnection and associated ionospheric fast flows before and during the TPA appearance and discuss how these ionospheric fast flows impinge on TPA formation.

This paper consists of six sections. The introduction and details of the instrumentation used in this study are given in sections 1 and 2. In section 3, the observational results of solar wind conditions monitored by GEOTAIL, auroral images from Imager for Magnetopause-to-Aurora Global Exploration (IMAGE), and the ionospheric flows and their patterns measured by Super Dual Auroral Radar Network (SuperDARN) High Frequency (HF) radars are reported. The observations by Cluster, related to the static TPA, are shown in section 4. Finally, in sections 5 and 6, we present a summary of our results, our discussion, and conclusions.

2. Instrumentation

The TPA was identified by simultaneous auroral observations by the Wideband Imaging Camera (WIC), which is part of the far ultraviolet (FUV) instrument (Mende, Heetderks, Frey, Lampton, Geller, Abiad, et al., 2000; Mende, Heetderks, Frey, Lampton, Geller, Habraken, et al., 2000; Mende, Heetderks, Frey, Stock, et al., 2000) onboard the IMAGE, launched in March 2000. WIC is used to image the aurora in a broad emissive spectral range between 140 and 190 nm at high spatial resolution with 2-min cadence.

It is important to understand TPA-associated plasma flows in the ionosphere to address how the TPA is formed and how ionospheric conditions associated with the nightside and dayside magnetospheric variations during the interval of the TPA appearance change. We therefore examined the ionospheric plasma flow data provided by the SuperDARN HF radars (Chisham et al., 2007; Greenwald et al., 1995). This radar array, located in the high-latitude regions in both Northern and Southern Hemispheres, provides line-of-sight measurements of ionospheric flow velocity. These measurements, obtained from nine SuperDARN radars in the Northern Hemisphere, have been used to produce high-latitude convection maps based on the "Map Potential" technique described by Ruohoniemi and Baker (1998). The line-of-sight velocity vectors are projected onto the geomagnetic (polar) grids and fitted to electrostatic potential solutions, which are described by a sixth-order spherical harmonic expansion. Complementary flow data from a statistical model characterized by upstream IMF conditions (Ruohoniemi & Greenwald, 1996) are used to constrain the large-scale flow pattern in regions where the radars provide no measurements (see Ruohoniemi & Baker, 1998, for details). All data procedures for the SuperDARN radar observations in this study are made by the software fitacf v1.2 and make_grid v1.14.er. It should be noted, however, that this statistical model provides only average ionospheric plasma flows that often do not correspond to varying ionospheric conditions, such as the evolution of TPAs (e.g., Chang et al., 1998). Thus, regions of little radar data coverage must be evaluated carefully.

The Cluster mission has been in operation since February 2001 (Escoubet et al., 2001) and comprises four identical satellites, flying in elliptical polar orbits with a period of about 57 hr. In this study, we utilize the magnetic and plasma data measured by the instruments onboard Cluster. Specifically, we examined the time variation spectra of electrons measured by the Plasma Electrons and Current Experiment (Fazakerley et al., 2010; Johnstone et al., 1997) and those of ions taken from Cluster Ion Spectrometer (Dandouras et al., 2010; Rème et al., 2001) which measures the ion fluxes irrespective of ion species in the energy range between 0.005 and 26.00 kev/q. The monitoring of the solar wind condition was made by GEOTAIL, which migrated from X = 28.05 R_E, Y = −5.47 R_E, and Z = 5.59 R_E to X = 28.61 R_E, Y = −4.41 R_E, and Z = 5.56 R_E in geocentric solar magnetospheric (GSM) coordinates in the upstream region during the TPA observational interval (about 1 hr 40 min). The IMF and solar wind plasmas were measured by the MaGnetic Field instrument (Kokubun et al., 1994) and Comprehensive Plasma Instrumentation (Frank et al., 1994), respectively.

3. Observational Results

3.1. Solar Wind Conditions

Figure 1 displays the solar wind conditions at the dayside magnetopause during about 3.3 hr between 6:00 and 9:20 UT. These solar wind parameters are plotted with a time shift of about 4 min, considering the traveling time from GEOTAIL to the dayside magnetopause position, which was yielded by average GEOTAIL position (GSM-X, GSM-Y, GSM-Z = 28.11, −5.35, 5.55 R_E) and average solar wind speed (V_{sw} = 509.2 km/s). We assumed the distance from the Earth to the dayside magnetopause nose as 10.5 R_E based on the Shue magnetopause model (Shue et al., 1998). From top to bottom, the panels show three components of the IMF in GSM coordinates, the clock angle between IMF-B_y and IMF-B_z components, $\theta_{CLOCK} = \tan^{-1}(\text{IMF-}B_y/\text{IMF-}B_z)$, and the solar wind dynamic pressure ($P_d = m_p N_p {V_{sw}}^2$), velocity (V_{SW}), and proton number density (N_p), respectively. The magenta and black horizontal broken lines show, respectively, "zero" and "middle value" axes in any given panel. As will be shown in section 3.2.1, a TPA started to appear at 7:28 UT, completely extended to dayside at 8:15 UT, and disappeared around 9:10 UT. The time interval bracketed by two light green broken lines is that of the solar wind conditions corresponded with the TPA growth and brightening as discussed in later sections.

All components of the field and plasma were fluctuating, but characteristic variations associated with, for example, interplanetary shocks or discontinuities, such as a heliospheric current sheet crossing, were not observed. For the presented interval, the IMF-B_z pointed northward throughout the whole interval, while the IMF-B_x had a dominantly antisunward component, and their average intensities remained unchanged (−4.0 and 2.5 nT). The clock angle values were also greater than −90° (being ~ −50°), indicating that northward and B_y (dawn-dusk) dominant IMF conditions were occurring during the TPA brightening.

The IMF-B_y component was dominantly negative (dawnward) for the first 2 hr from 6:00 UT to 8:20 UT, although IMF-B_y briefly changed its polarity to duskward around about 7:10 UT. It also had perturbations to the polarity changes between −1.0 and +2.0 nT after 8:15 UT.

All plasma parameters, such as the solar wind dynamic pressure, velocity, and density, were stable during the presented 3.3 hr. Their average values were 1.7 nPa, 510 km/s, and 3.8/cc, respectively, which were not extreme solar wind conditions, although only the solar wind velocity was faster than the average solar wind speed (~ 400 km/s).

3.2. TPAs and Associated Ionospheric Flows: IMAGE and SuperDARN Radar Observations

3.2.1. Brightening of the TPAs

Figure 2 displays 12 selected snapshots of a series of the stages from the growth of the TPA to the TPA disappearance via its brightening in the Northern Hemisphere. These panels comprise the brightening of the main nightside auroral oval, the onset of the TPA, the TPA (crossbar) part protruding from nightside auroral oval to the dayside, the TPA brightening, and weakening (disappearance) as detected by the FUV-WIC onboard the IMAGE satellite. We have reduced the dayglow contaminations as much as possible by setting the imager view software provided from the FUV-WIC team to the glow removal mode. The crossbar part of the TPA and its growth fluxes are highlighted by blue ovals in Figure 2. We confirmed that the TPA-associated fluxes started to appear at 7:27:48 UT, when we define as the time of "TPA onset," and the TPA persisted for about 1 hr 40 min (~ 9:10:04 UT). Each image is projected onto magnetic latitude (MLat)-magnetic local time

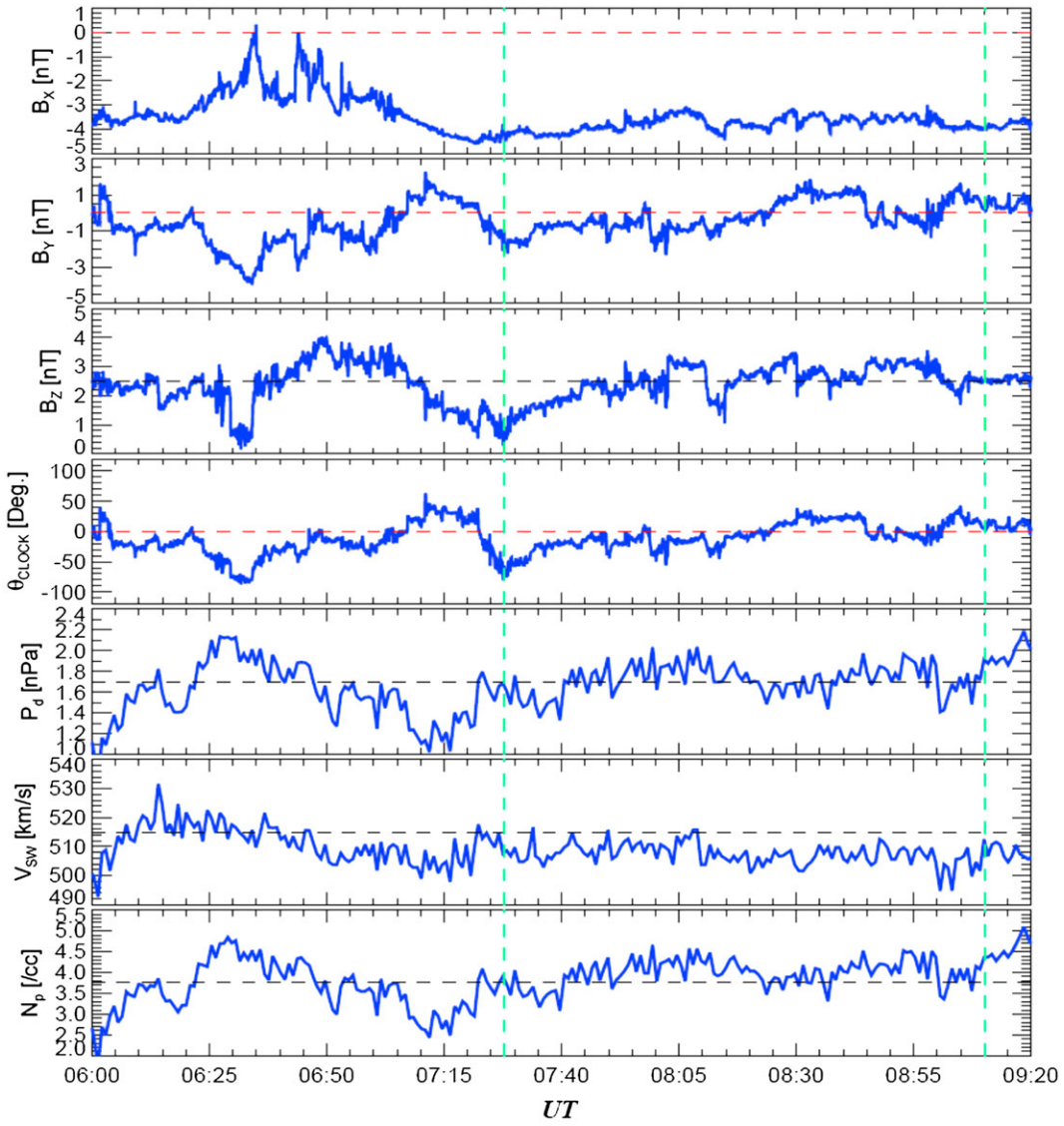

Figure 1. The solar wind conditions at the dayside magnetopause for about 3.3 hr monitored by GEOTAIL are displayed with about 4-min time shift. From top to bottom panels, three components of interplanetary magnetic field (IMF) in geocentric solar magnetospheric coordinates, the clock angle between IMF-B_y and IMF-B_z components $\left(\theta_{\mathrm{CLOCK}} = \tan^{-1}\left(\frac{\mathrm{IMF-B_y}}{\mathrm{IMF-B_z}}\right)\right)$, solar wind dynamic pressure (P_d), velocity (V_{SW}), and proton number density (N_p) are shown, respectively. The solar wind condition interval corresponded with a focused transpolar arc signature is bracketed by two light green broken lines. UT = geocentric solar magnetospheric.

(MLT) coordinates. The upper and lower sides in each figure show the dayside and nightside whose MLT is 12 and 24 h (0 h), respectively. The dawn (6 MLTs) and dusk (18 MLTs) meridians correspond to the right and left sides, respectively. The color code is assigned according to the number of photons (the intensity of brightness) in units of Rayleigh.

After the onset of the TPA (7:27:48 UT), it clearly evolved and intensified in brightness in the dawnside but had no discernible motion (drifting). The "boundary" between the oval and TPA was obscure during the TPA growth, and the TPA was aligned to the auroral oval. In particular, from 7:27:48 to 7:58:29 UT, the TPA was growing from the nightside and aligned to the dawnside main auroral oval. The TPA completely connected to the dayside after 8:14:51 UT (hereafter, refer to as TPA brightening). The luminosity in the nightside part of the TPA and auroral oval was particularly intense, from 8:29:10 to 8:47:34 UT. After 8:55:45 UT shown in Figure 2j, the TPA luminosity became weaker and finally disappeared on 9:10:04 UT (Figure 2l). The full set of

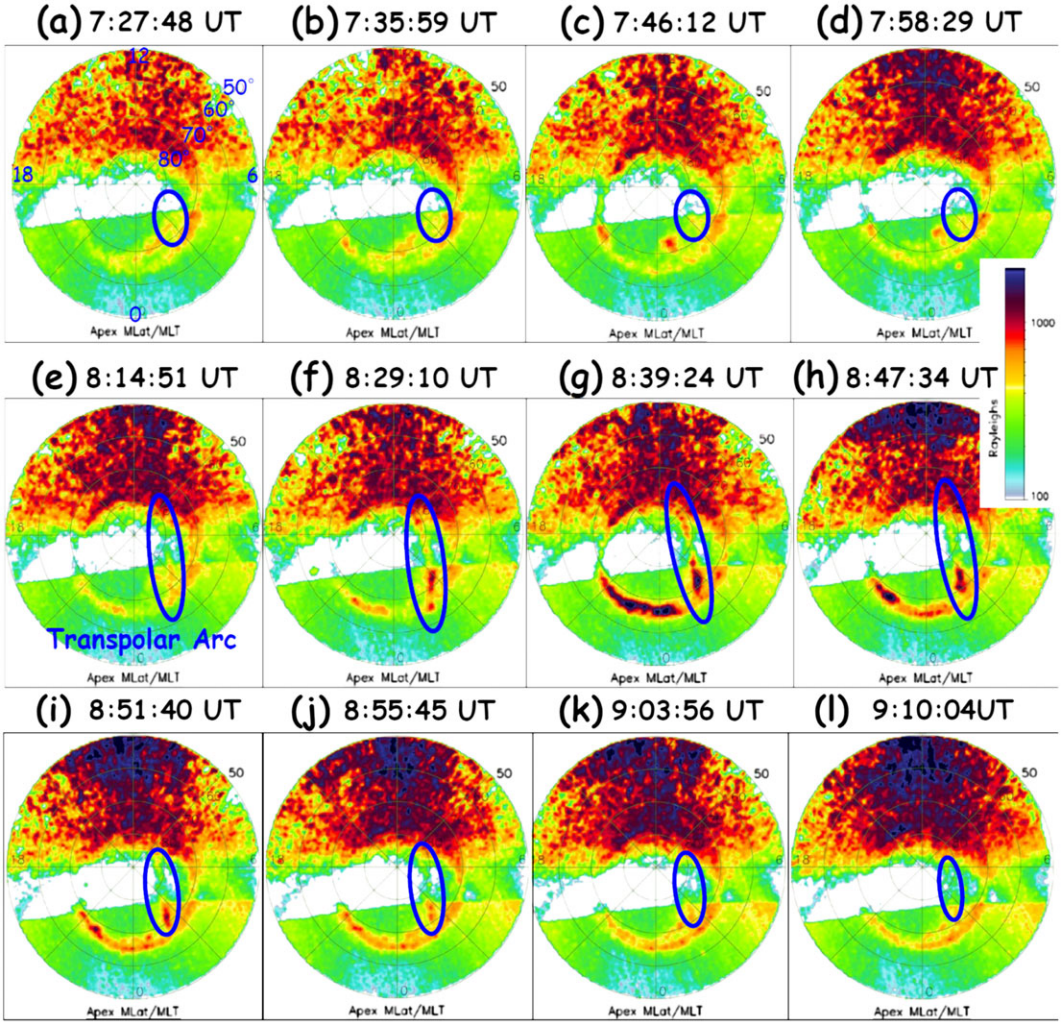

Figure 2. Selected 12 snapshots of the aurora ovals and transpolar arcs in the Northern Hemisphere in polar coordinates detected by the far ultraviolet (FUV) Wideband Imaging Camera (WIC) onboard Imager for Magnetopause-to-Aurora Global Exploration. The top and bottom sides in each figure show the noon and nightsides whose magnetic local time (MLT) is 12 and 24 h (0 h), respectively. The dawn (6 MLTs) and dusk (18 MLTs) meridians correspond to the right and left sides, respectively. The color code is assigned according to the flux of auroral electrons in units of Rayleigh. The transpolar arc brightening is marked with blue ovals. Possible dayglow contaminations were removed by setting Imager for Magnetopause-to-Aurora Global Exploration FUV-WIC data view software provided by the FUV-WIC team to the glow removal mode.

FUV-WIC image data spanning 2 hr between 7:20 and 9:20 UT, when the main theta auroral oval, TPA growth, and complete connection to the dayside were observed, can be seen as Movie S1, provided in supporting information. The appearance of the TPA on the dawnside of the polar cap is consistent with the solar wind conditions as shown in Figure 1, particularly the predominant dawnward orientation of the IMF-B_y component before the TPA appearance.

3.2.2. Ionospheric Flow Profiles at the TPA Onset and During the Growth of the TPA

We will now discuss SuperDARN radar observations of the ionospheric plasma flows and their variations before and during the TPA formation and those associated with the TPA brightening in this section. The ionospheric flows before the TPA appearance and after the TPA onset are important signatures in order to examine whether or not magnetotail reconnection was related to the TPA formation mechanism. We therefore investigate the ionospheric plasma flow vector data obtained from the SuperDARN radars. Figure 3 presents the Northern Hemisphere ionospheric plasma flow streamlines and "E × B" drift velocity vectors (from 18 to 6 h in MLT) during the TPA preonset interval from 7:00 to 7:26 UT and the TPA growing interval from 7:27 to

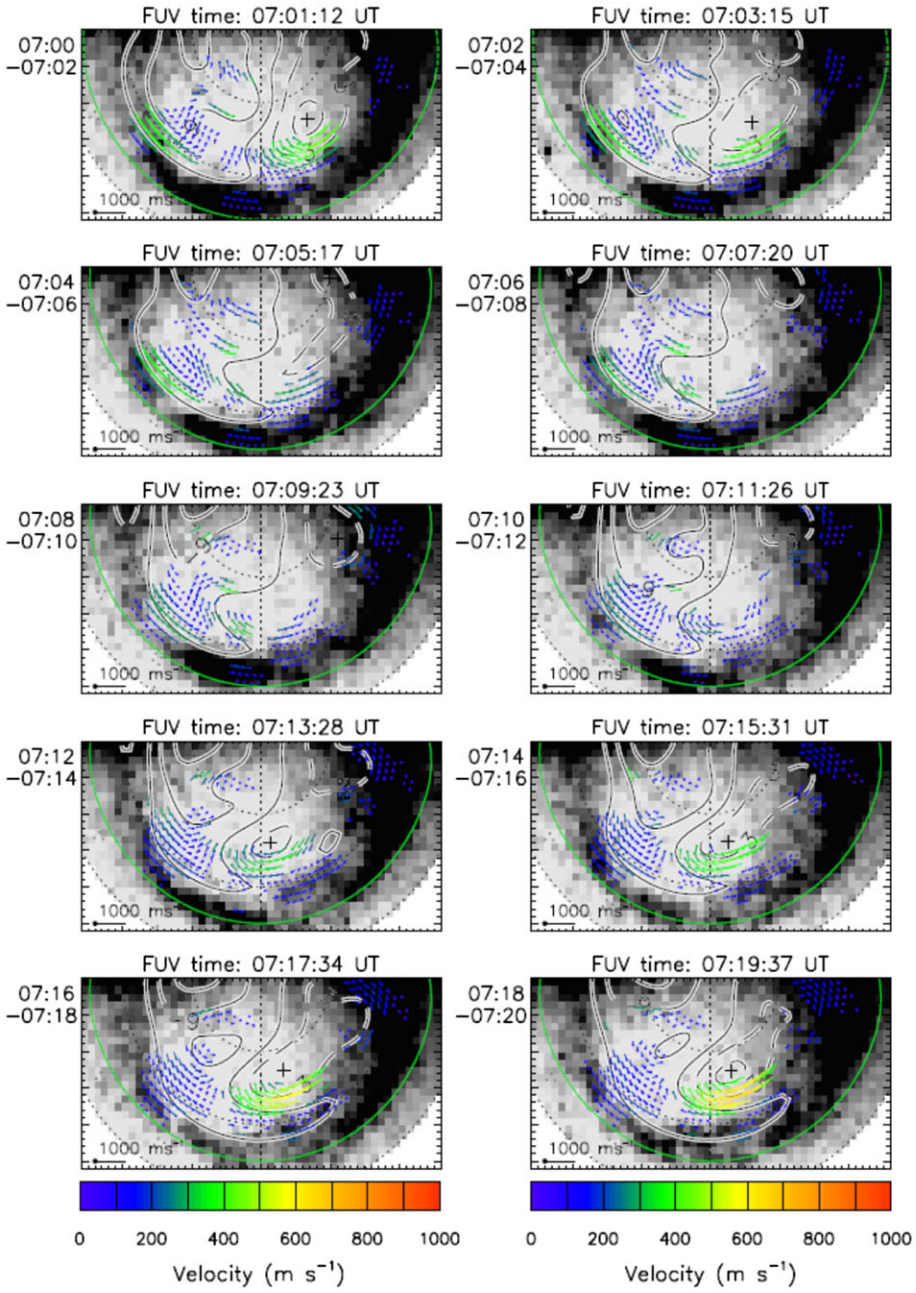

Figure 3. (a–c) The nightside ionospheric flow streamlines and their line-of-sight velocity vectors measured by Super Dual Auroral Radar Network radars in the Northern Hemisphere, overlaid by the far ultraviolet-Wideband Imaging Camera (FUV-WIC) data from Imager for Magnetopause-to-Aurora Global Exploration, are shown during 1 hr between 7:00 and 8:00 UT before the transpolar arc (TPA) appearance and during the growth of the TPA. The dotted circles in each panel are indicated the magnetic latitude (MLat) lines from 60° to 80°. The left, bottom, and right sides in each panel show 18, 24, and 6 h in magnetic local time, respectively. The time resolutions of the Super Dual Auroral Radar Network and Imager for Magnetopause-to-Aurora Global Exploration FUV-WIC data are 2 min. These streamlines and velocity vectors are projected onto the geomagnetic grids, and positive (maximum) and negative (minimum) electrostatic potential models, controlled by the IMF conditions as shown with black solid and broken curves. The green curves show the Heppner-Maynard boundary, which is the lower latitude limit for the ionospheric plasma convection pattern. The vector length and color code are assigned according to the flow orientation and intensity of ionospheric velocity in units of meter per second. Westward ionospheric fast flows, which are key phenomenon in explaining the TPA formation based on nightside magnetic reconnection, are marked with blue ovals. The bulge structures, which were located along poleward boundary of the nightside auroral oval, are indicated and marked by magenta ovals.

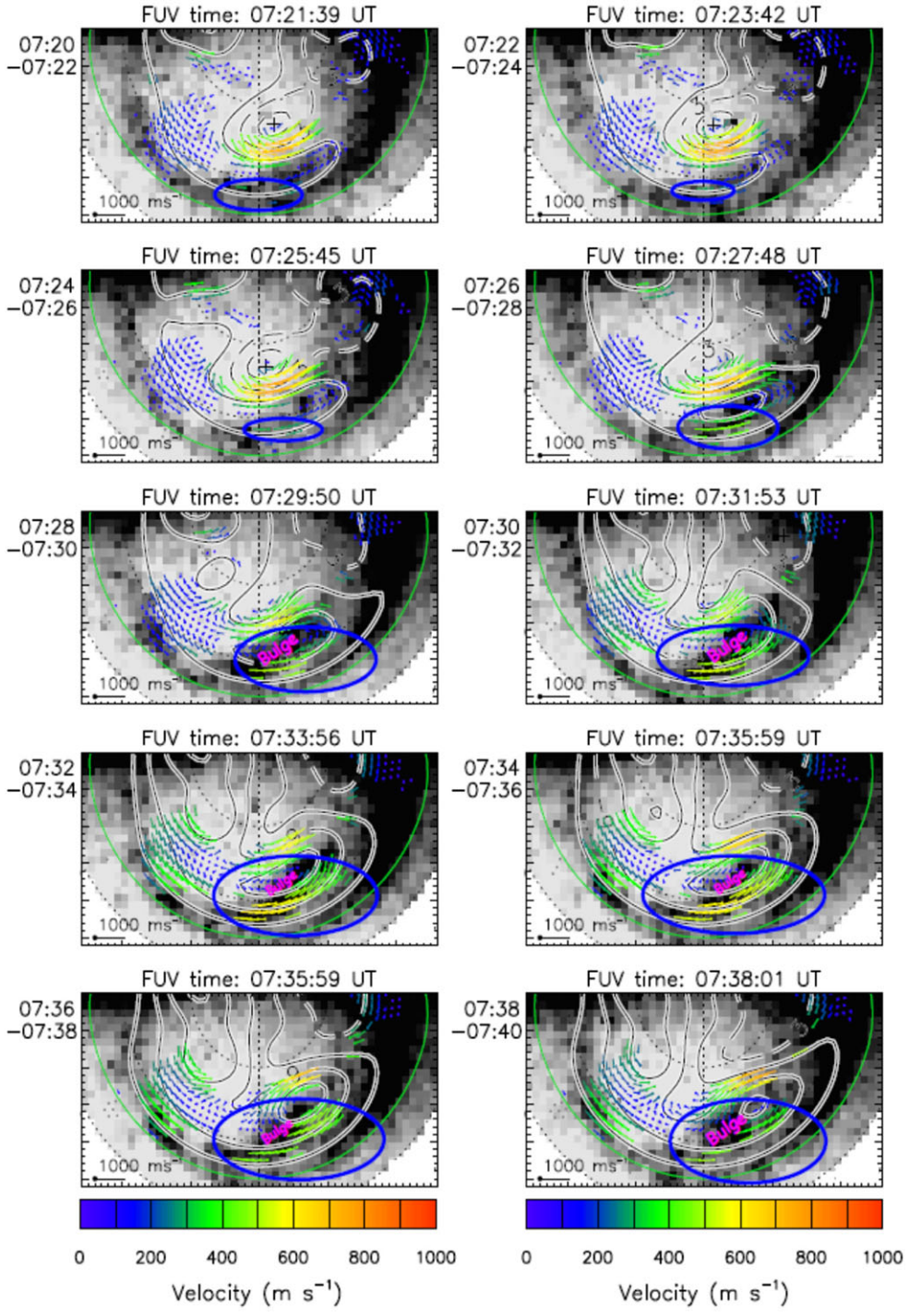

Figure 3. (continued)

8:00 UT with a time step of 2 min. The left, bottom, and right sides in each panel correspond to 18, 24, and 6 h in MLT, respectively. The dotted semicircles indicate the MLat range between 60° and 80°. We also overlay these flow velocity profiles onto the corresponding IMAGE FUV-WIC auroral imager data with 2-min time resolution. Black indicates higher auroral luminosity, and the IMAGE observational time is shown on the top in each panel. The overlaid plots of the SuperDARN backscatter and the IMAGE auroral imager during about 2 hr between 7:20 and 9:20 UT are provided in supporting information. This interval includes the whole TPA growth (between 7:27:48 and 8:12:48 UT) and brightening (from 8:14:51 to 9:10:04 UT) stages.

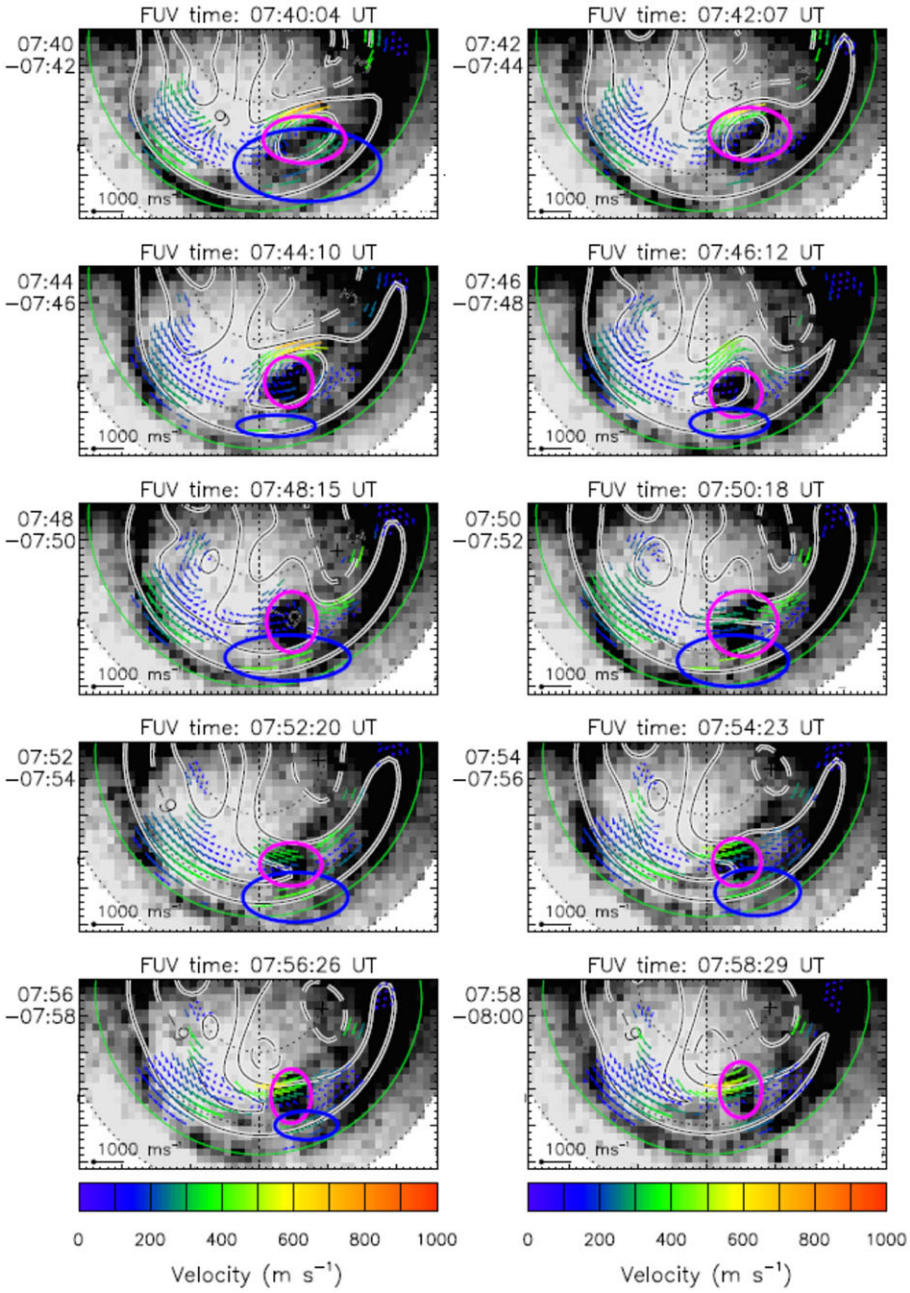

Figure 3. (continued)

The equipotential streamlines and their values are shown with black solid and broken contours on the duskside and dawnside, respectively. This distinction is made because the signs of ionospheric electrostatic potential in the dawnside and duskside are opposite; the electric potential at dawn is positive (maximum potential denoted by a plus sign) and at the dusk is negative (minimum denoted by a cross). The large-scale electric field direction, of course, is the same in the two hemispheres, pointing from dawn to dusk across the polar cap. The green curves show the lower-latitude limit of the ionospheric plasma convection pattern (Heppner & Maynard, 1987), determined from the line-of-sight ionospheric plasma velocities measured by the radars. Each dot in the panels shows a SuperDARN radar measurement. The length of the vectors and color code is assigned according to the flow orientation and intensity of ionospheric velocity in units of meter per second.

Before the appearance of the TPA (the TPA onset), the nightside main aurora oval was well defined. No significant ionospheric flow patterns can be found from 7:01:12 to 7:19:37 UT on the midnight auroral oval (closed flux tube), but weak plasma flows with the range around 0.3 km/s began to be seen on midnight auroral oval from 7:21:39 UT as shown by blue ovals. Even during the growth of the TPA after the TPA onset, the ionospheric westward plasma flows, ranging between 0.3 and 0.65 km/s, were locally (although noncontinuously) observed equatorward of the poleward edge of the midnight sector main auroral oval between 7:28 and 7:40 UT and again between 7:44 and 7:55 UT. These flows are highly suggestive of accelerated plasma confined within the closed flux region of the nightside auroral zone and are one of the characteristic signatures of "tail reconnection during IMF northward and nonsubstorm intervals (TRINNIs)" (Grocott et al., 2004, 2003). The fastest TRINNI events, detected in the nightside auroral oval in this interval, had velocity components between than 0.4 and 0.7 km/s. Compared with the TRINNI flows which were reported by Grocott et al. (2003, 2004, 2005), this velocity range was slower. The westward direction of these flows is consisted with that expected for TRINNIs when IMF-B_y is negative. During the intervals when the ionospheric TRINNI flows were observed (particularly, from 7:36 to 8:00 UT), the TPA-associated closed fluxes also seem to split off from near the dawnside main auroral oval and grow to the dayside. However, they were not associated with significant drifting motion to duskward. Similar TPAs aligned to the main auroral oval had already been reported and identified by Kullen et al. (2002), who classified such events as "oval-aligned" arcs and proposed that their formations would be related to the thickness or twist of the magnetotail plasma sheet (Makita et al., 1991). However, Kullen et al. (2015) also found that oval-aligned arcs were also associated with ionospheric TRINNI flows predicted by the Milan et al. (2005) reconnection mechanism. In our case, the ionospheric TRINNI flows were observed when the TPA was growing, aligned to the dawnside main auroral oval. Therefore, nightside reconnection should play a significant role in the formation of the TPA observed, which is consistent with the results by Kullen et al. (2015).

After 7:29:50 UT, a flux "bulge" structure had been seen on the poleward edge of the midnight sector main auroral oval (~1 MLT) during the TPA growth interval, but interestingly, this structure was absent when the TPA started to brighten (after 8:14:51 UT). Plasma flows were directed along the poleward edge of the bulge, and these flows formed a vortex structure along the rim of this bulge, in particular, seen at 7:35:59 and 7:40:04 UT. However, as the tip of the TPA was close to the dayside from 7:48:15 to 7:58:29 UT (see Figures 2 and 3c or Movie S1 in the supporting information), eastward ionospheric flows entered this bulge and oriented themselves along the TPA.

The origin of ionospheric TRINNI flows is near the eastward edge of the nightside auroral brightening point where the TPA is formed. Siscoe and Huang (1985), Grocott et al. (2003, 2004, 2005), Milan et al. (2005), Fear and Milan (2012b), and references therein point out that these return flows should originate in a flow across the open/closed polar cap boundary, if they are driven by tail reconnection. In many panels of Figure 3, there is clear evidence for eastward flow poleward of the auroral oval that then rotates across the poleward boundary to form the westward return flows. The vortex flows along the rim of the bulge were also directed toward the TPA and crossed the poleward edge of the main auroral oval (TRINNI flow region), rotating from an eastward to a westward direction. These flows are thus a very probable signature of magnetotail flux closure, which is key to the TPA formation mechanism of Milan et al. (2005).

The presence of TRINNI flows without a large-scale coincident TPA process, as illustrated in Figures 3b and 3c, is consistent with an unencumbered return of closed flux following magnetotail reconnection. In the panels near 8:00 UT (Figure 3c), it can be seen that these flows begin to subside. This is also consistent with the notion of a TPA resulting from closed flux "getting stuck," which by definition should be accompanied by an absence of return flows arising from the sector which maps to the TPA.

Figure 4 shows a SuperDARN radar data plot, superimposed onto the IMAGE FUV-WIC data on 7:27:48 UT, the time at which the TPA started to grow. We defined this as the time of TPA onset as shown in Figure 2a. The plasma flows which rotate along the poleward edge of the bulge from eastward to westward are observed just poleward of the auroral oval, at the same MLT sector as that of the TPA formation as marked with a magenta oval. Furthermore, these flows have an equatorward velocity component, directed antisunward along the TPA. At the same time, the speed of return flows seems to be reduced when changing their orientations from eastward to westward; rather than the newly closed flux being "returned" to the dayside by the characteristic TRINNI flows, it is instead stagnating somewhat within the TPA, which begins to build up and

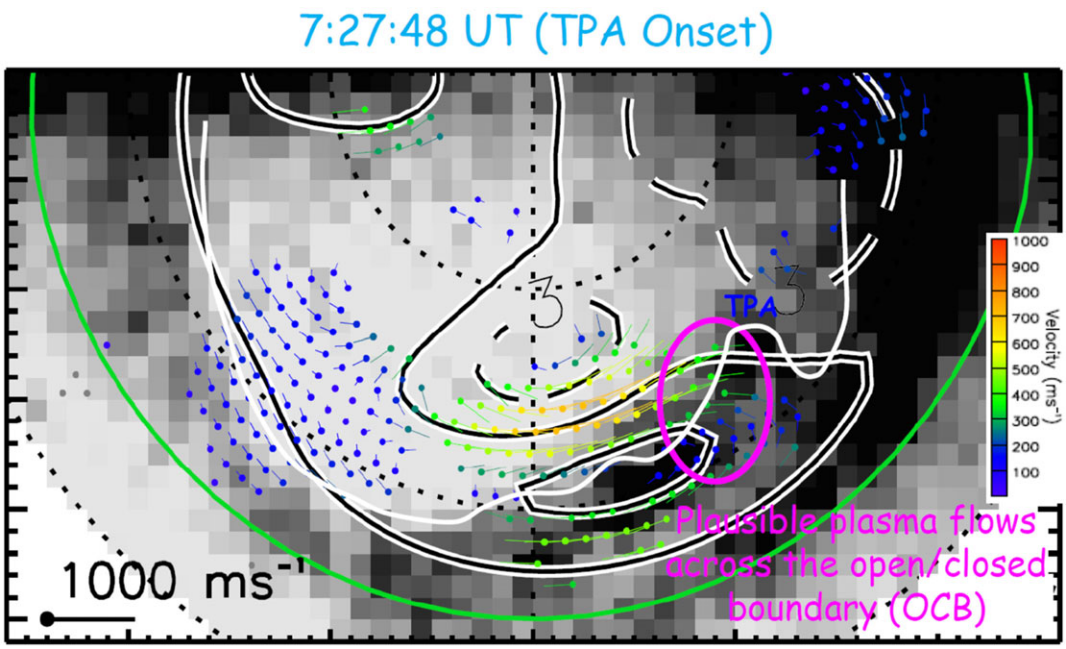

Figure 4. An overlaid plot of Super Dual Auroral Radar Network radar and Imager for Magnetopause-to-Aurora Global Exploration far ultraviolet-Wideband Imaging Camera data on the transpolar arc (TPA) onset (7:27:48 UT) is shown. Slow plasma flows, which rotate from eastward to westward direction as marked with magenta oval, which are plausibly part of a flow pattern across the open/closed polar cap boundary, were observed at the same magnetic local time sector as that of the TPA growth. These slow flows are evidence for a contribution of magnetotail reconnection to the formation of the closed flux tube developing toward the dayside (polar) region, that is, the TPA formation. The white curve shows the poleward boundary of the nightside main auroral oval and the TPA protruding (tip) part as determined with the visual inspections.

protrude deeper into the lobe, mapping further across the polar cap toward the dayside (e.g., Fear et al., 2014, 2015).

3.2.3. TPA-Associated Ionospheric Flow Profiles

In order to examine how the observed TPA was associated with the ionospheric flows, we compare the ionospheric velocity maps obtained from the SuperDARN radar measurements after the TPA onset with IMAGE FUV-WIC data, onto which the northern hemispheric SuperDARN velocity profiles are overlaid in Figure 5. The white curve shows the approximate poleward boundary of the nightside main auroral oval and the TPA protruding (tip) part (as particularly shown in Figures 5a and 5b), which are determined by the visual inspection of IMAGE FUV-WIC imager data. We found the poleward boundary of the midnight auroral oval to be located over a MLat range of between 68° and 70°.

Westward and eastward ionospheric plasma flows with a broad range between 0.4 and 0.75 km/s were seen in all panels. Further flows were distributed at latitudes higher than the poleward edge of the nightside oval (~ 75°). This implies that they are not associated with the nightside (midnight sector) main auroral oval and TPA, suggesting that they were not flowing inside the closed flux region formed by the magnetotail reconnection process. Instead, they appear to circulate within the polar cap, suggesting that they are related to a stirring of open flux that has previously been associated with TPA motion (Milan et al., 2005). In Figures 5a and 5b which show the flow profile during the TPA growth, evidence for magnetotail reconnection is provided by the ionospheric return flows across the open/closed polar cap boundary and TRINNI flows on the nightside auroral oval. However, even during the TPA growth interval, these characteristic ionospheric flows associated with nightside reconnection were only weakly observed as shown in Figure 5c and were not observed in Figure 5d, suggesting that the ionospheric TRINNI flows were not always seen continuously and at the same flow intensity level. During the intervals when the TPA started to brighten and disappeared (weakened), which are displayed from Figure 5e to 5l, no clear evidence for flows associated with magnetotail reconnection are found.

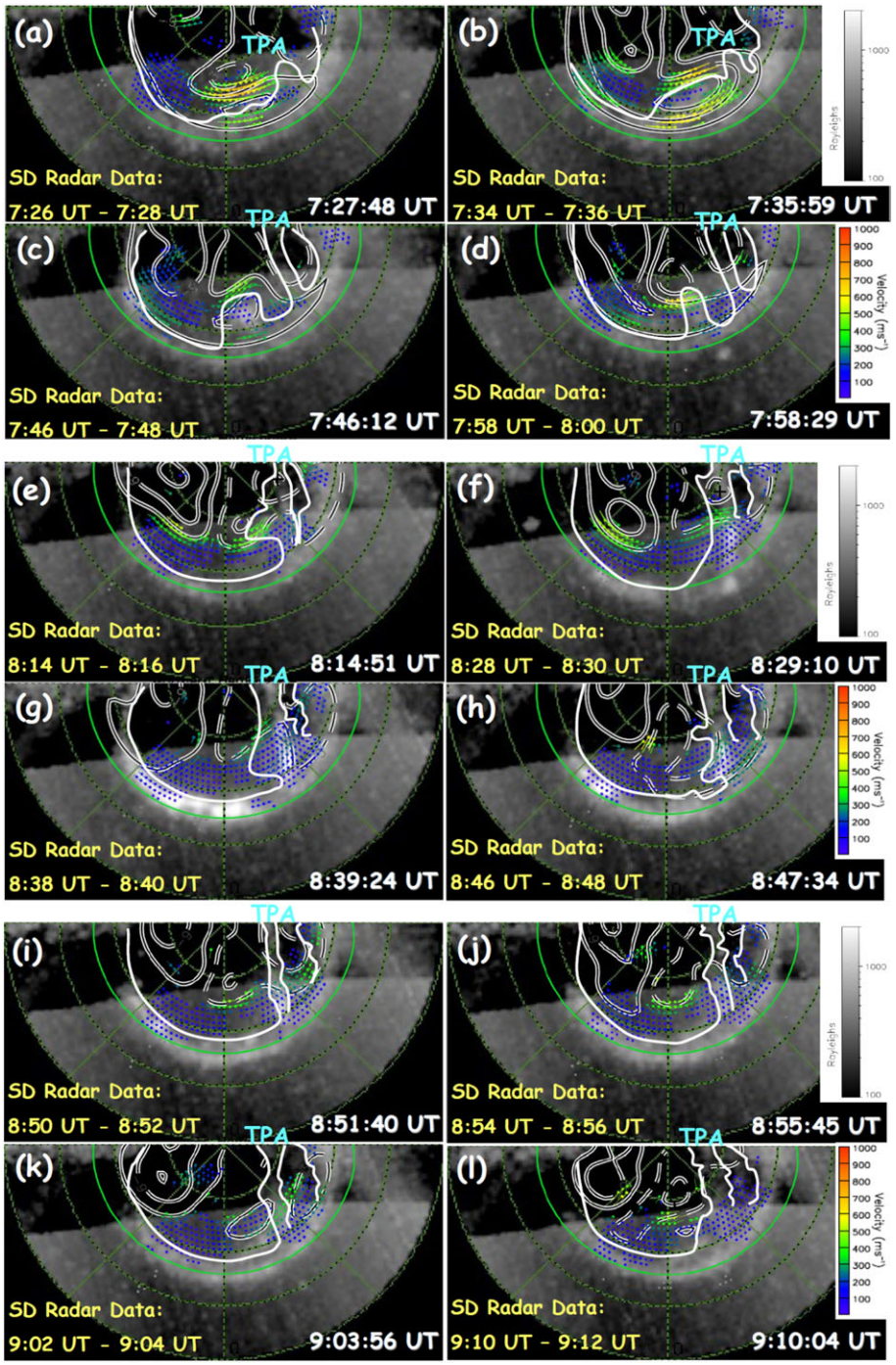

Figure 5. (a–l)Twelve overlaid plots of the ionospheric flow streamlines and their line-of-sight velocity vectors measured by Super Dual Auroral Radar Network radars, overlaid by the far ultraviolet-Wideband Imaging Camera (FUV-WIC) data from IMAGE, are shown. The Imager for Magnetopause-to-Aurora Global Exploration (IMAGE's) aurora snapshot times and figure format are the same as those in Figure 2. The time intervals of each panel in the Super Dual Auroral Radar Network data are 2 min. The white curves show the approximate poleward boundary of the nightside main auroral oval and the TPA protruding (tip) part (as particularly shown in panels a and b), which are determined by the visual inspection of IMAGE FUV-WIC imager data.

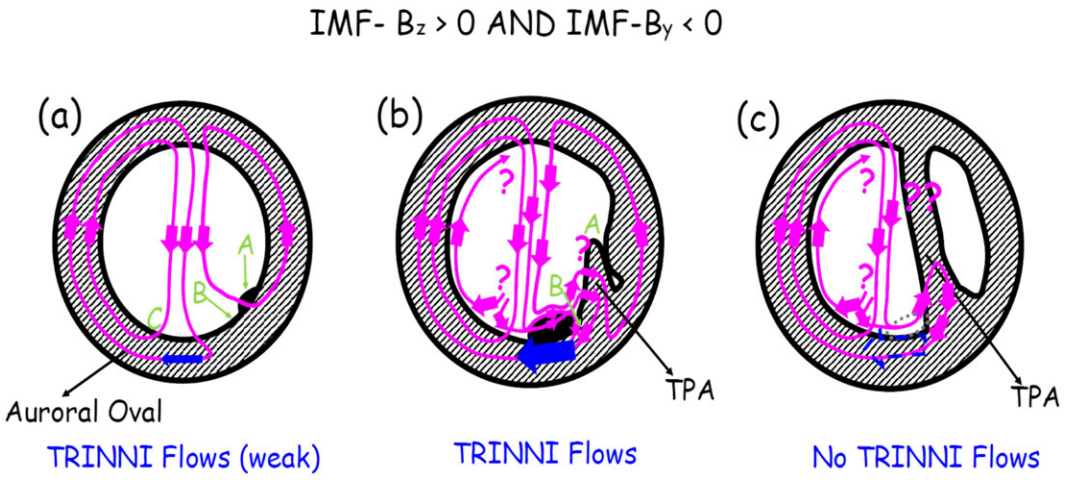

Figure 6. The schematic diagrams for the ionospheric convection patterns and tail reconnection during interplanetary magnetic field (IMF) northward nonsubstorm intervals (TRINNI) flows at the three stages of the transpolar arc (TPA) growth under the conditions of IMF-$B_z > 0$ and IMF-$B_y < 0$ are displayed: (a) before and the onset of the formation of the TPA, (b) during the TPA growth to the dayside region, aligned to the dawnside auroral oval, and (c) after the complete formation of the TPA (TPA brightening). The shaded area and magenta curves show the auroral oval and ionospheric flow patterns, respectively. The westward ionospheric TRINNI flows are shown with blue arrows in panels (a) and (b). See the detailed discussions in the text.

One might suggest that an absence of the ionospheric TRINNI flows during the TPA brightening could be interpreted as a cessation of the magnetotail reconnection process. However, compared with the ionospheric profiles during the TPA growth and before the TPA onset as shown in Figure 3, the ionospheric TRINNI flows were seen on closed flux tubes, being evidence that nightside reconnection has proceeded. As seen in the IMAGE FUV-WIC imager data in Figures 2 and 5, the TPA (closed flux tubes formed by magnetotail reconnection) clearly evolved and grew to the dayside. Furthermore, the connection point between the nightside main auroral oval and the TPA was clearly brightening even after the TPA completely connected to the dayside. Therefore, in this case, we could infer that the flows associated with magnetic reconnection were present during the TPA brightening, that is, after the TPA completely connected to the dayside region, even without the ionospheric TRINNI flows.

Figure 6 shows the schematic diagrams for the ionospheric convection patterns at the three stages of the TPA growth under the northward and duskward (IMF-$B_z > 0$ and IMF-$B_y < 0$) IMF conditions. The shaded area and magenta curves show the auroral oval and ionospheric flow patterns, respectively, and the figure indicates three spatial locations (A, B and C). The weak westward ionospheric TRINNI flows near 0.3 km/s were found in the midnight sector of the auroral oval just before the TPA started to form (point A) as shown with a thin blue arrow in Figure 6a. However, at this stage, no return flows were observed.

During the growth interval of the TPA (Figure 6b), both clear TRINNI flows and return flows across the open/closed polar cap boundary were observed at point B, which was close to point A. The TPA would grow aligned to the dawnside main auroral oval. Furthermore, a flux bulge was formed near point B. The plasmas were flowing across the open/closed boundary along poleward edge of the bulge structure and circulated further within the polar cap region (including the vortex flows within the bulge). Further eastward plasma flows were heading for the TPA through the bulge structure as the TPA grew to the dayside. The field lines which were closed to point A should stagnate to form the TPA rather than the ionospheric TRINNI flows. Within the polar cap region on the duskside, sunward plasma flows leading from the premidnight sector were also observed. Because coverages of poleward of polar cap and the dayside regions of the SuperDARN backscatter were not sufficient, it remains observationally unclear whether or not the plasma flows along poleward edge of the bulge entered the tip of the growing TPA or how the duskside sunward plasma flows circulated. At the intervals when the TPA was forming (particular Figure 6b), the fact that TRINNI flows persist suggests that there is closure of flux that does not map to the newly forming TPA (at point A), since any such flux will stagnate, rather than forming part of the ionospheric TRINNI flows as discussed above in section 3.2.1. This implicitly shows that the extent of the nightside reconnection line is wider than the thickness of the TPA at formation.

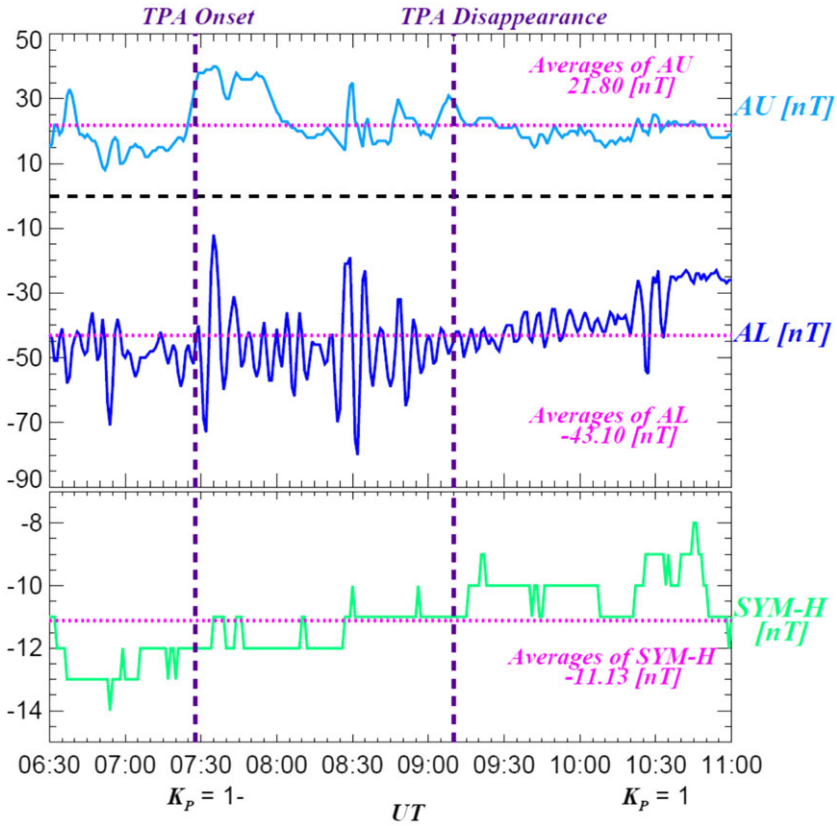

Figure 7. Geomagnetic conditions associated with the transpolar arc (TPA) brightening are displayed. From top to bottom panels, *AU*, *AL*, and *SYM-H* (which approximately shows the geomagnetic activity at middle and low latitudes), during 4.5 hr between 6:30 and 11:00 UT, are shown, respectively. During the presented time interval, the *AL* index shows extremely clear oscillations and has particular large-amplitude waves within the TPA interval. The other *AU* and *SYM-H* indices did not have wavy variations. The average values of each parameter and associated K_p index are also indicated in the panels and the bottom of these panels, respectively. The TPA interval is bracketed by two thick purple broken lines.

Even after the TPA has completely formed (shown in Figure 6c), we suggest that magnetotail reconnection should be continuing because the joint part of the nightside end of the TPA and the main auroral oval brighten as shown in particular in Figures 2e–2l. We infer from the flows that the reconnection process is occurring away from the nightside auroral oval but in the vicinity of the TPA. For that reason, the ionospheric TRINNI flows have subsided and the flows across the midnight sector of the auroral oval may be nonexistent. Instead of these flows, the ionospheric convection flows (which form neither TRINNI flows nor return flows) enter and are subsumed into the TPA. As there were no accompanying TRINNI flows at that time, we assume that the continuation of magnetotail reconnection occurred over an extent comparable to the TPA width. Even during the TPA brightening interval, sunward ionospheric plasma flows leading from the premidnight sector, just poleward of the duskside polar cap, were observed.

3.3. Geomagnetic Field Variations Associated With TPA

Figure 7 shows the observed variations of three geomagnetic activity indices, *AU*, *AL*, and *SYM-H* (which approximately shows the middle- and low-latitude geomagnetic activities), during 4.5 hr between 6:30 and 11:00 UT. The time intervals bracketed with two thick purple broken lines are the main TPA interval (from the onset to the disappearance of the TPA) discussed earlier. Geomagnetic activity was relatively low including when the TPA appeared, as evidenced by the K_p index which ranged from −1 to 1, indicating that the orientation of IMF-B_z component during the TPA brightening had been northward.

The amplitude of the *AU* variations before the TPA onset (7:27:48 UT) was smaller than that after the appearance of the TPA. During the interval of the TPA growth and brightening, the *AU* value showed no significant variations, although it displayed some enhancements. The average *AU* value was 21.8 nT. The associated *AL*,

whose average value was −43.1 nT, showed extremely clear oscillations during the whole interval. These *AL* oscillations are consistent with the observation of small-amplitude perturbations in the Pi2 range at high latitudes during the TRINNI flows (Grocott et al., 2003). Particularly, large amplitude oscillations between −85 and −20 nT were also seen, indicating that the auroral current variations were higher in association with an appearance of the TPA.

SYM-H, whose average value was −11.13 nT, did not show significant variations, compared with the *AL* index, suggesting that ring current did not significantly develop in association with the TPA. This absence of the ring current development is also indicative of a nonmagnetic storm/substorm near or during the TPA interval. We also checked whether or not a substorm onset occurred by investigating Pi2 waves from geomagnetic field variations recorded at low-latitude smagnetic observatories, but clear Pi2 waves were absent (not shown here). From these ground geomagnetic observations, it can be concluded that our TPA occurred during a nonstorm and nonsubstorm interval.

4. Cluster Observations Tailward of the Cusp in the Northern Hemisphere Associated With the TPA

4.1. Cluster Location Relative to the TPA

In the previous sections, we investigated the ionospheric flows that would lead to TPA formation based on the nightside reconnection model. Furthermore, the detailed relationship between magnetotail reconnection occurrence and the ionospheric flows was examined. In this section, we discuss how high-latitude lobe reconnection impinges on the TPA based on Cluster measurements at the cusp region. According to the nightside reconnection TPA formation model, high-latitude lobe magnetic reconnection plays a significant role in governing TPA motion (Milan et al., 2005); it is not associated with the formation of the TPA but can interact with the closed flux forming the TPA leading to a net opening of magnetic flux by the lobe reconnection process (Fear et al., 2015). If the tip of the TPA is far from the location of the cusp, it should drift toward the cusp due to the convection excited by the lobe reconnection process (Milan et al., 2005). On the other hand, if the TPA is already near the cusp region, then it has limited scope for motion and should be static (Fear et al., 2015; Fear & Milan, 2012a). Our TPA had been static from its appearance to fading, so the static nature of our TPA might be interpreted based on lobe dynamics and relative distance between the TPA and cusp region.

Figure 8 shows the footpoints of the Cluster 1 (C1) probe trajectory from 8:00 to 9:25 UT with a time step of 5 min in Geomagnetic Coordinates. The C1 footpoint was calculated based on the Tsyganenko (1989) magnetic field model (T89) under geomagnetic conditions of K_p = 1 and solar wind dynamic pressure of P_{dyn} = 2 nPa. We compared two additional magnetic field models proposed by Tsyganenko (1995, 2002) with the T89 model, but there was no significant difference between the three models in this case. The Cluster footpoints are superimposed on IMAGE FUV-WIC data from 8:31:13 UT when the TPA was brightening. The strong dayside glow contaminations, where the brightness was extremely high, are reduced by scaling each horizontal stripe separately. From these removals of the dayside glows, MLat of the open/closed dayside polar cap boundary of the main auroral oval can be identified around 80°. The white broken curve shows the poleward boundary of the dayside main auroral oval and the duskward boundary of the TPA. In the case of the frame shown, this recovers the TPA structure at its sunward edge. The TPA seems to grow to the dayside from 2 MLT, where it started to form, to near the noon section from 10 to 11 MLT. Considering the relation between the cusp location and the IMF orientation, between 7:23 and 8:23 UT, the IMF-B_y component was negative (dawnward) as shown in Figure 1. The cusp, thus, is expected to be located at the prenoon (dawnward) sector (e.g., Frey et al., 2002), which would mean a proximity to the tip of the TPA. The arc tip moved after 8:29 UT slightly toward the noon sector (see Figure 2f). This is because the TPA slightly drifted as the cusp location moved to postnoon (duskward) sector due to a positive IMF-B_y component between 8:24 and 8:46 UT according to Figure 1.

The footpoint of C1 traveled poleward in the dayside magnetosphere, moving from ~11:30 to ~13:30 MLT, inclined slightly to a magnetic meridian line from 8:00 to 9:25 UT as shown with orange crosses. In particular, at 8:50 UT, C1 approached and crossed the cusp region because its location was the point whose MLat was around 75°, and MLT range was between 12 and 13. At this time, Cluster detected reconnection signatures tailward of the cusp under changeable IMF-B_y polarity between 8:49 and 8:52 UT, in which we will discuss in section 4.2.

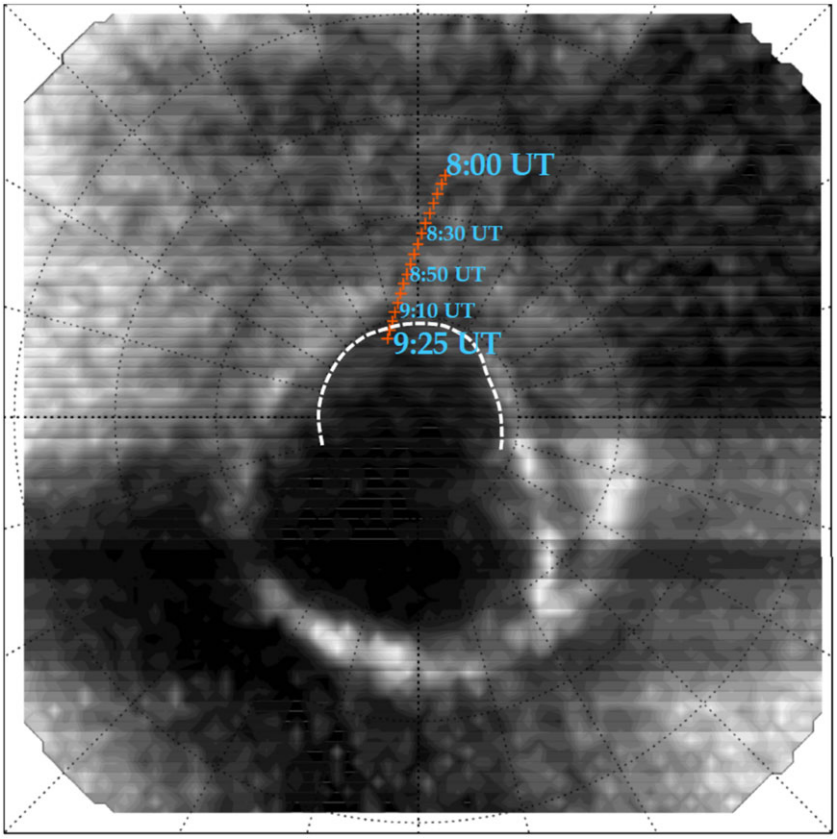

Figure 8. An overlaid plot of the transpolar arc (TPA) detected by the Imager for Magnetopause-to-Aurora Global Exploration far ultraviolet-Wideband Imaging Camera on 8:31:13 UT when the TPA was brightening and footprint trajectory of the C1 probe between 8:00 and 9:25 UT with a 5-min step, calculated based on Tsyganenko 89 model (Tsyganenko, 1989) under geomagnetic conditions of K_p = 1 and P_{dyn} = 2, is displayed. The dayglow contaminations are reduced by scaling each horizontal stripe, separately. By gathering the horizontal slice images, the sunward edge TPA structure is clearly emergent. The white broken curve shows the poleward boundary of the dayside main auroral oval and the duskward boundary of the TPA.

In the next section, we report the signatures of tailward of the cusp reconnection in detail based on the temporal variation for the plasma energy flux from Cluster.

4.2. Temporal Variations of Electron Energy Flux

Figure 9 shows (a) electron and (b) ion energy-time (E-t) spectrograms, which show the temporal variations of the electrons and ions, for the Cluster passage tailward of the cusp measured by the Plasma Electrons and Current Experiment and Cluster Ion Spectrometer instruments onboard C1.

C1 approached and crossed the cusp region in the Northern Hemisphere at MLat ~ 75° (MLT ~ 12.5 h) from the dayside magnetosphere to the magnetotail lobe. Based on these electron and ion spectrograms shown in Figures 9a and 9b, we suggest that C1 passed the cusp during a period of reconnection tailward of the cusp. Furthermore, zoomed-in E-t spectrograms during 15 min between 8:40 and 8:55 UT, when C1 observed structures of "plasma (electron and ion) edges," which are an indicative (indirect) signature of magnetic reconnection (e.g., Gosling et al., 1990), are shown in the bottom four panels. Unfortunately, no SuperDARN radar scatter along or nearby the track of C1 was found. In this case, therefore, the C1 measurements cannot be supported and explained by the ionospheric flow profiles as obtained from the ground-based observations.

In the electron E-t spectrograms, at the onset time of the TPA brightening (~ 8:15 UT), C1 was still at the outer edge of the dayside plasma sheet region but observed two populations of different energy plasmas. The black curves (indicated by the thick black arrow in selected panels) in the spectrograms indicate the spacecraft potential level; therefore, the components below 10.0 eV are the populations of photoelectrons that

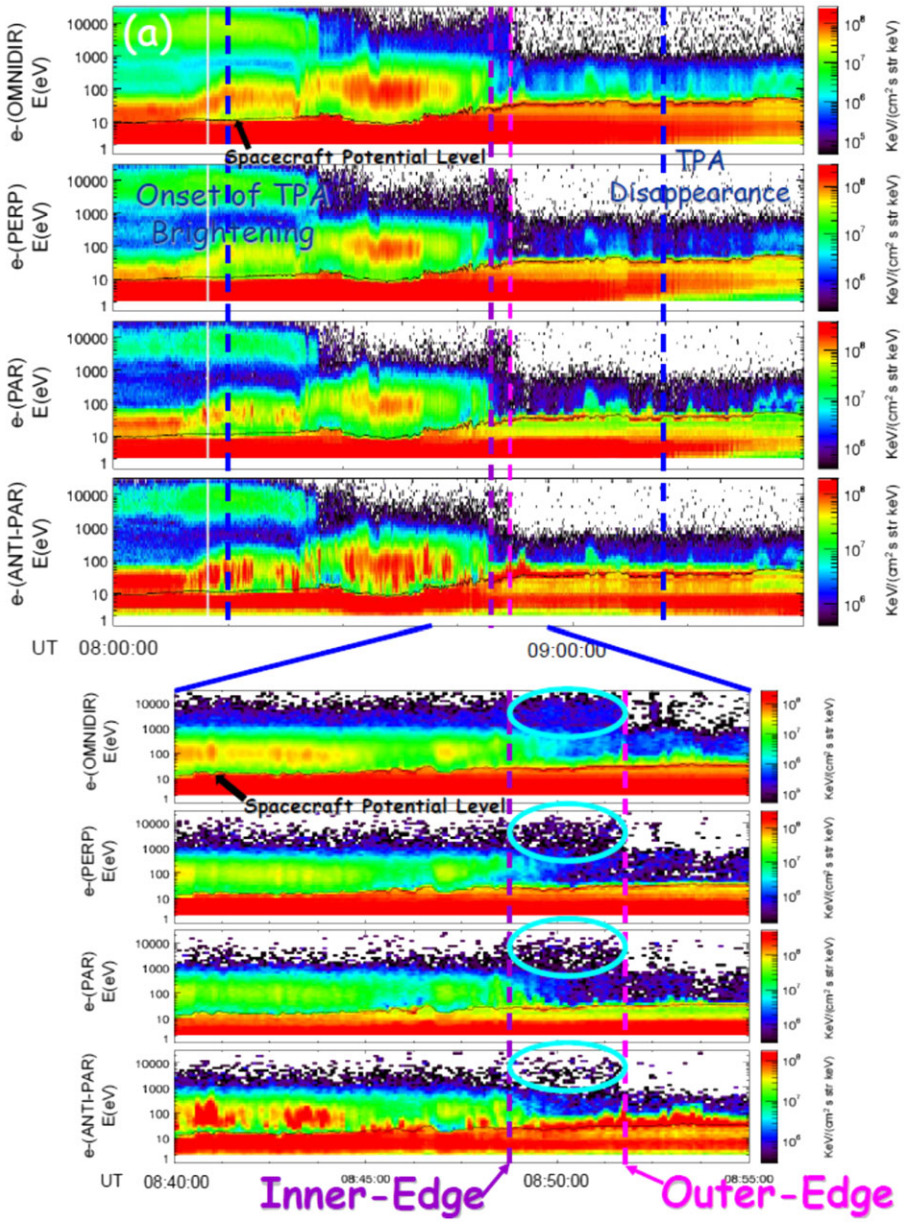

Figure 9. (a) The spectrograms for the temporal variations of the electron energy (E-t spectrograms) measured by the PEACE instrument onboard C1 are displayed. The top four panels show the E-t spectrograms in the omnidirection, perpendicular, parallel, and antiparallel pitch angle directions during 1.5 hr between 8:00 and 9:30 UT. Zoomed-in spectrograms during 15 min between 8:40 and 8:55 UT are also displayed in lower four panels. The vertical axis gives the energy of the electrons (in eV), and the universal time (UT) is shown in the horizontal axis. The color code is assigned according to the particle differential energy flux in units of kev/(cm^2 s str kev). An ~1-hr interval between 8:15 and 9:10 UT, corresponding to when the transpolar arc was brightening, that is, the transpolar arc was completely connected to the dayside, is bracketed by blue broken lines. The electron edge structure formed by high-latitude lobe reconnection is bracketed by dark purple and magenta broken lines. The black curves as marked by the thick black arrows in the upper and the first of the lower set spectrograms show the spacecraft potential level, and the population below this level indicates that of the photoelectrons, released from the surface of satellite. (b) The spectrograms for the temporal variations of the electron energy (E-t spectrograms) measured by the Cluster Ion Spectrometry instrument onboard C1 are displayed. All figure formats are the same as Figure 9a.

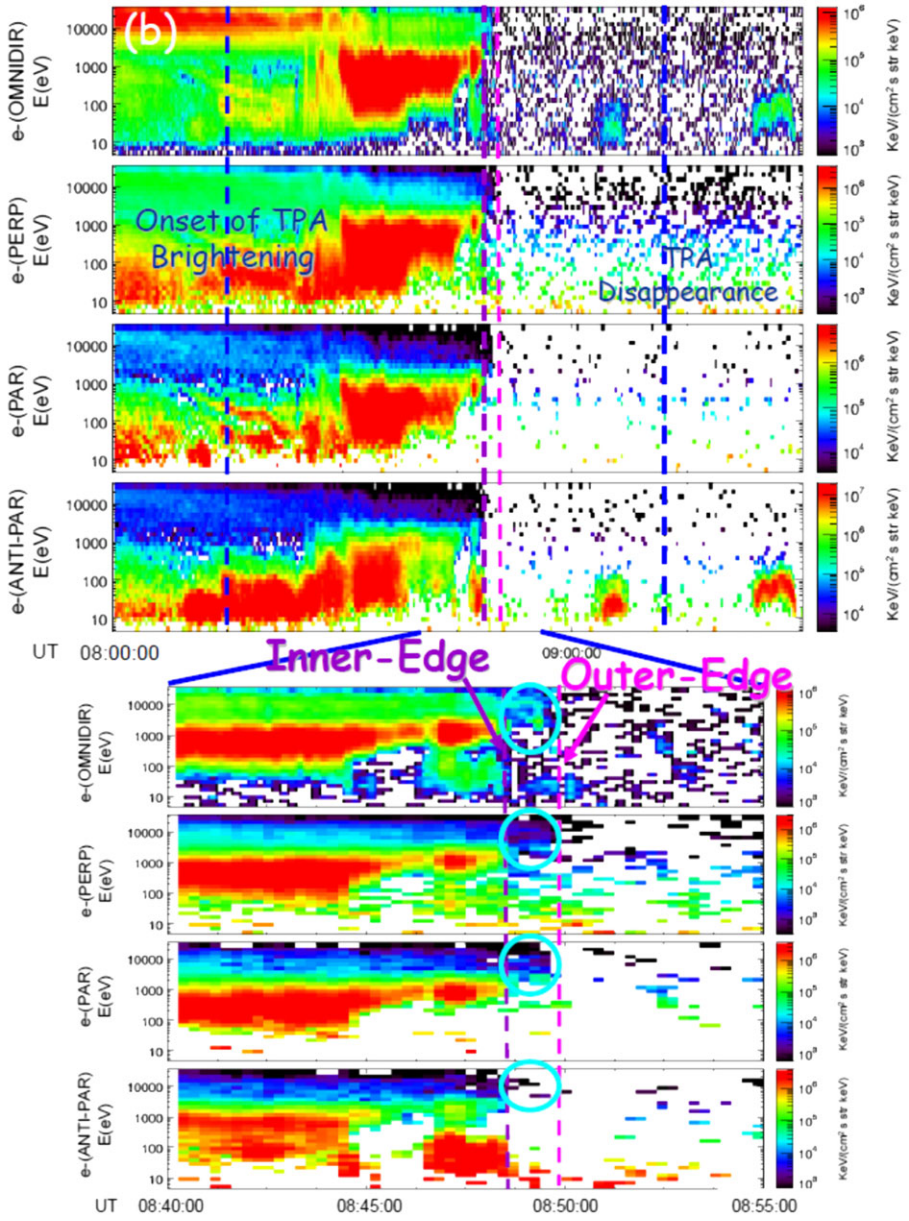

Figure 9. (continued)

were released from the surface of satellite. C1 mainly observed plasma typical of the cusp region with a broad energy range between 30.0 eV and 1.0 keV, which is an intermediate energy range between plasma of magnetospheric origin and the solar wind. The dayside plasma sheet components higher than 10.0 keV and the medium energy ions from the cusp ranging between 40 eV and 4.0 keV were also observed in the associated ion E-t spectrograms.

In addition to this component, more tenuous and energetic electrons and ions, covering the electron and ion energy ranges between 1.0 and 10.0 keV and between 2.0 and 20.0 keV, were seen. In the zoomed-in E-t diagram, the two plasma regimes with the different energy range were distinguished particularly in the perpendicular (second panel) and parallel (third panel) directions. From around 8:49 UT, labeled as "inner edge," the flux of main cusp plasmas started to decrease, and the cusp components became a "minor" component at about 8:52 and 8:50 UT in the electron and ion fluxes, respectively (labeled with "outer edge") as bracketed by dark purple and magenta broken lines. Interestingly, as marked with cyan ovals, the flux of associated tenuous and high-energy components remained even though the main cusp plasma populations gradually

decreased over about 3 min in the fluxes of electrons and 1 min in ion flux. The population of these energetic components, however, was not present after 8:52 and 8:50 UT in the electron and ion fluxes, respectively.

During these several minute intervals between about 8:49 and 8:52 UT, we believe that C1 observed a manifestation of magnetic reconnection tailward of the cusp region and associated "plasma edge structure," because high-energy and tenuous plasma components, whose ion and electron flux levels are ~ 10.0 and ~ 5.0 keV, respectively, prevailed during this period. This "edge structure" of plasmas at the inner side of the magnetopause, which was formed by reconnection, is an indicative (indirect) signature of magnetic reconnection at the magnetospheric boundary regions (Gosling et al., 1990; Øieroset et al., 2015). Also in our observation, as marked with cyan ovals, an electron and ion edge, identified as the "inner-most point," where the solar wind components accelerated by reconnection can penetrate into the magnetosphere along the open field lines or perpendicular to the local field lines at the magnetopause, was observed. The observation shows that the outer edge of an "electron edge" was formed outside that of an "ion edge," suggesting that an electron edge was distributed more extensively tailward than an ion edge. The tenuous and high-energy plasmas were the accelerated component at the electron and ion edge (as bracketed by dark purple and magenta broken lines) formed by magnetic reconnection tailward of the cusp.

Even though C2 and C4 were located close to C1 with the distance less than 1 R_E, the profiles of the E-t diagram, when crossing the cusp region from the dayside to tail lobe regions, were different from that of C1 (not shown here). Only C1 detected the clear boundaries of plasma energy variations between the cusp, dayside plasma sheet and tail lobe region, and clear "plasma edge" signature. The separation of the Cluster spacecraft was such that C1, C2, and C4 were at higher altitude than C3, separated by about an Earth radius in GSM-Z. The footpoints of the three higher-altitude spacecrafts (C1, C2, and C4) were close with each other (within 3,000 km), but the C1 orbital footprint lay slightly more dawnward than those of the other two. From these plasma structures, we might estimate that observed cusp reconnection was either a "localized" phenomenon or the trio of higher-altitude Cluster spacecraft "clipped" the duskward edge of the cusp.

Our interpretation, therefore, is that Cluster observed the cusp plasma structure and an indicative (indirect) signature for magnetic reconnection tailward of the cusp when it approached and crossed the cusp region. This case differs from that of Fear et al. (2014, 2015), where Cluster did not observe the in situ signature of high-latitude lobe reconnection (which was inferred from the auroral observations) but did observe the plasma structure associated with the TPA.

5. Summary and Discussion

In this study, we have investigated the ionospheric flow profiles before and during the observation of a TPA which remained on the dawnside for 1 hr on 16 September 2001. The IMF-B_y and IMF-B_z orientations before and during the TPA appearance were dawnward and northward.

The ionospheric flow patterns (in particular, flow patterns in the nightside) are closely associated with TPA formation. The ionospheric fast plasma flows were observed just equatorward of the poleward edge of the midnight sector of the main auroral oval, that is, in the region of closed flux, prior to the TPA onset determined by IMAGE FUV-WIC data. They are the ionospheric return flows associated with the so-called TRINNIs, reported by Grocott et al. (2003, 2004) and Milan et al. (2005), and are evidence for the occurrence of nightside magnetic reconnection. Slower flows that appear to cross the open/closed polar cap boundary at the MLT where the TPA started to grow were also observed, indicating that magnetic field lines were being closed by nightside reconnection in this region. These flow profiles and patterns show that nightside reconnection plays a significant role in this TPA formation (Fear & Milan, 2012b; Milan et al., 2005). On the contrary, it also seemed that the TPA obscurely appeared due to a "splitting off" from the main auroral oval in the dawnside (particularly see Figures 2a and 2b). However, this detachment was associated with the ionospheric flow signatures due to magnetotail reconnection (e.g., ionospheric TRINNI and return flows), being consistent with previous results by Kullen et al. (2015).

We should note that the dayglow contaminations of IMAGE FUV-WIC data in this event were too strong to completely remove the dayglow's influence in IMAGE FUV-WIC data. Therefore, it is insufficient to draw final conclusions about exactly how the TPA was formed based on the auroral imager data alone. Combining the nightside ionospheric flow patterns measured by the SuperDARN radars with the IMAGE FUV-WIC data, we

point out that the TPA observed was oval-aligned arc, and its formation was closely related with magnetotail reconnection. Therefore, the obtained results are also in agreement with the statistical results of Fear and Milan (2012b) and Kullen et al. (2015), who confirmed the validity of the nightside reconnection model proposed by Milan et al. (2005) for all types of TPA.

Milan et al. (2005) and Fear and Milan (2012b) showed cases where the ionospheric TRINNI flows on closed flux had been observed not only before but also during the TPA growing and brightening. According to the TPA formation model proposed by Milan et al. (2005), the TPA would be formed by a protrusion of the closed flux tubes, which are generated by nightside reconnection, from the main auroral oval in the premidnight or postmidnight section into the polar cap toward the dayside. Therefore, the continuation of TRINNI flows throughout the lifetime of the TPA, in the events reported by Milan et al. (2005) and Fear and Milan (2012b), indicates that the reconnection process persisted during the interval in which the TPA was observed. However, in our case, the ionospheric TRINNI flows comparable to the cases observed by Grocott et al. (2003, 2004) and Milan et al. (2005) were observed just before and during the TPA growth period, but they then subsided during the period of the TPA brightening, that is, the time coinciding with the TPA becoming completely connected to the dayside. There are three possible explanations for the lack of TRINNIs during the period of observation of the TPA brightening itself. The first is that the flows existed but did not give rise to backscatter detected by the SuperDARN radars. We suggest that this is unlikely given the amount of low-velocity backscatter, being present close to the region of interest. The second possibility is that magnetotail reconnection might have ceased at the point where the TPA stops growing to the dayside any further, that is, the TPA completely connected to the dayside oval, as shown in Figure 6c. However, auroral brightening is still observed at the point of connection between the TPA and the oval at several times (i.e., Figures 2g and 2h and 5g and 5h), being suggestive of reconnection continuity. We propose that a third possible scenario may be due to the extent of the reconnection site in the magnetotail. At any stage where the TPA is either growing or has finished forming, we would only expect TRINNI flows if the reconnection lines map to a wider extent of the nightside auroral main oval than the TPA; this is because the TPA is associated with a region of newly closed flux which stagnates and remains stuck in the magnetotail, mapping into the polar cap. The TRINNI flows, which are inherent to the Milan et al. (2005) mechanism, are actually formed by field lines adjacent to the TPA and which consequently do not stagnate. Therefore, we would expect TRINNI flows to be absent if the extent of the reconnection line is comparable to that of the TPA. Newly closed field lines will contribute either to the closed wedge of flux forming the TPA or to the ionospheric TRINNI flows, depending on its location, so if the magnetotail reconnection line is comparable in length to the width of the TPA, there may not be an accompanying TRINNI signature as discussed with Figure 6 (see section 3.2.3).

The nightside reconnection TPA formation model proposed by Milan et al. (2005) postulates that high-latitude lobe reconnection plays no role in the formation of TPAs, but it does control the azimuthal motion of the TPA in the ionosphere. Fear et al. (2015) argue that field line topology changes caused by reconnection tailward of the cusp (which normally simply stirs lobe flux without a topology change) are introduced by the presence of a TPA. The distance between the TPA and cusp region (where magnetic reconnection occurs) would determine whether or not the TPA is "static" or "dynamic," because a TPA should drift toward the cusp as a result of the lobe reconnection process, if the TPA location was away from the cusp (Fear et al., 2015). In our case, the Cluster measurements did not map exactly to the TPA but were made at the cusp region, possibly on its duskward edge as noted above, and located about 3 h in MLT duskward of the sunward tip of the TPA (Figure 8). Furthermore, the relative location between the Cluster footpoints and the auroral imager data (shown in Figure 8) indicates that the TPA had been located near the cusp region since it appeared. Through detection of the electron edge structure, our observations also revealed that magnetic reconnection was occurring at the high-latitude magnetopause, tailward of the cusp. Statistical studies report the longitudinal extent of the cusp to be of the order of 2–4 h in MLT (Bogdanova et al., 2006; Newell et al., 1989; Pitout et al., 2006), so it is highly feasible that the TPA intersects the dawnward side of the cusp as the Cluster spacecraft passes through its dawnward side. Therefore, we could interpret the static nature of our TPA in the dawn-dusk direction based on lobe dynamics, and relative distance between the TPA and cusp region, proposed by Milan et al. (2005) and Fear et al. (2015).

Figure 10 shows a schematic diagram, projected onto the magnetic meridian plane, for a Cluster passage tailward of the cusp during reconnection from the dayside to lobe region. If high-latitude lobe reconnection formed plasma edge structures, where reconnection-accelerated plasmas enter (or escape to) the inside

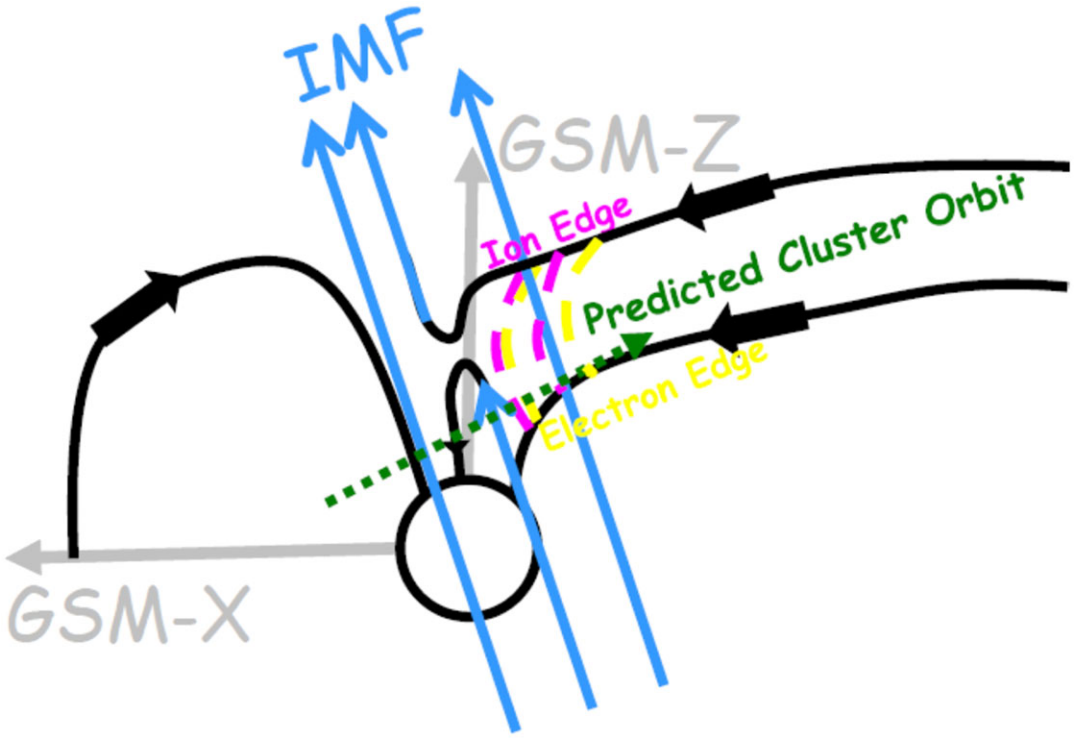

Figure 10. A schematic diagram, projected onto the magnetic meridian plane, for high-latitude lobe region during which Cluster would pass plasma edge structures as shown with green dotted line, formed by tailward of the cusp magnetic reconnection, from the dayside to lobe region is illustrated. The regions surrounded by two magenta and yellow broken curves are ion and electron edges, respectively. The thick blue arrows and black curves display the interplanetary magnetic field (IMF) and magnetospheric field lines, respectively. GSM = geocentric solar magnetospheric.

(outside) of the magnetospheric boundary region along the open field line and perpendicular to the local field line, the outer edge of an electron edge (the region between two yellow broken curves) should be present tailward of an ion edge (the region surrounded by two magenta broken curve) due to the time-of-flight effect (e.g., Bogdanova et al., 2006; Gosling et al., 1990; Øieroset et al., 2015).

Finally, in this study, we cannot directly estimate FACs using the magnetic field and particle flux data taken from the satellites flying over the low-latitude region, such as DMSP (Defense Meteorological Satellite Program), FAST (Fast Auroral Snapshot Explorer), CHAMP (Challenging Minisatellite Payload), and Ørsted satellites because unfortunately, no lower-altitude satellites passed directly over or nearby the TPA, and large data gaps were found in other satellites on this day. If the plasma and magnetic field data could be obtained from these series of the low-latitude orbiting satellites, we would reveal the detailed current structures and particle precipitation profiles of the TPA observed. In future work, it also remains to try to precisely and quantitatively evaluate the FACs based on the magnetic field data obtained from low-altitude satellite fleets.

6. Conclusion

In this study, we investigated the profiles of the ionospheric flows, such as the TRINNI and return flows across the open/closed polar cap boundary, before and during the growth and brightening of the TPA with 1 hr duration based on ground-based observations. The relationship between the TPA and IMF conditions and contributions of nightside and dayside magnetic reconnections to the TPA physics were discussed based on both ground- and space-based observations. The following items are the main results obtained through this study.

1. The TPA was observed in the dawnside during dominant northward IMF-B_z and negative IMF-B_y intervals under stable solar wind conditions. This relationship between TPA location and IMF conditions was consistent with the results obtained from statistical studies made previously.

2. Just before and during the growth of the TPA, the ionospheric fast plasma flows (ionospheric TRINNI flows) were found in the midnight sector of the main auroral oval, suggesting that ionospheric plasmas were accelerated and confined to the closed flux tubes by magnetotail magnetic reconnection.
3. Slower "return" plasma flows across the open/closed polar cap boundary, which are a phenomenon indicative of closed field line formation due to nightside reconnection, were seen at the same MLT as the location of the TPA formation point. These results suggest that magnetotail magnetic reconnection played an essential role in the formation of the TPA.
4. Our results suggest that the fate (absence or presence) of the ionospheric TRINNI flows on closed field lines during the interval of TPA formation (growth) would be closely related with the scale of magnetotail reconnection.
5. The static nature of the TPA could be interpreted by lobe dynamics and the relative distance between the TPA and cusp region, proposed by Milan et al. (2005) and Fear et al. (2015); the dayside tip of a static TPA should be located near the cusp region.

Acknowledgments
This work is supported by the National Natural Science Foundation of China (grants 41574157, 41322031, 41404131, and 41628402). M. N. thanks Yonglian Zhang, Zhiguan Yuan, Hui Zhang (IGGCAS), and Huishan Fu for useful and constructive discussions. A. G. was supported by STFC grant ST/M001059/1. R. C. F. was supported by STFC Ernest Rutherford Fellowship ST/K004298/2. IMAGE FUV-WIC data can be obtained by contacting the corresponding author (M. N.) or can also be accessed from http://image.gsfc.nasa.gov. The SuperDARN radars are funded by the research agencies of Australia, China, Canada, France, Italy, Japan, South Africa, the UK and the United States. SuperDARN data are freely provided for scientific research purposes and can be obtained by contacting the authors (M. N. and A. G.) or any of the SuperDARN PI research groups (http://www.superdarn.ac.uk). All SuperDARN radar data are processed by the software fitacf v1.2 and make_grid v1.14.er. Cluster CIS and PEACE data can be obtained from the Cluster Science Archive (https://www.cosmos.esa.int/web/csa), provided by ESA. GEOTAIL MGF and CPI data can be taken from Data ARchives and Transmission System (DARTS), provided by the Center for Science-satellite Operation and Data Archive (C-SODA) at ISAS/JAXA (http://darts.isas.jaxa.jp/about.html.en) and Coordinated Data Analysis Web (https://cdaweb.sci.gsfc.nasa.gov/index.html/), provided by GSFC/NASA. We also thank the World Data Center for Geomagnetism, Kyoto University, for accessing the data of K_p, *AU*, and *AL* indices from http://wdc.kugi.kyoto-u.ac.jp/index.html.

References

Bogdanova, Y. V., Owen, C. J., Fazakerley, A. N., Klecker, B., & Rème, H. (2006). Statistical study of the location and size of the electron edge of the low-latitude boundary layer as observed by Cluster at mid-altitudes. *Annales de Geophysique*, *24*, 2645–2665. https://doi.org/10.5194/angeo-24-2645-2006

Chang, S.-W., Scudder, J. D., Sigwarth, J. B., Frank, L. A., Maynard, N. C., Burke, W. J., et al. (1998). A comparison of a model for the theta aurora with observations from Polar, Wind, and SuperDARN. *Journal of Geophysical Research*, *103*(A8), 17,367–17,390. https://doi.org/10.1029/97JA02255

Chisham, G., Lester, M., Milan, S. E., Freeman, M. P., Bristow, W. A., Grocott, A., et al. (2007). A decade of the Super Dual Auroral Radar Network (SuperDARN): Scientific achievements, new techniques and future directions. *Surveys in Geophysics*, *28*(1), 33–109. https://doi.org/10.1007/s10712-007-9017-8

Cumnock, J. A. (2005). High-latitude aurora during steady northward interplanetary magnetic field and changing IMF B_y. *Journal of Geophysical Research*, *110*, A02304. https://doi.org/10.1029/2004JA010867

Cumnock, J. A., Sharber, J. R., Heelis, R. A., Blomberg, L. G., Germany, G. A., Spann, J. F., & Coley, W. R. (2002). Interplanetary magnetic field control of theta aurora development. *Journal of Geophysical Research*, *107*(A7), 1108. https://doi.org/10.1029/2001JA009126

Cumnock, J. A., Sharber, J. R., Heelis, R. A., Hairston, M. R., & Craven, J. D. (1997). Evolution of the global aurora during positive IMF B_z and varying IMF B_y conditions. *Journal of Geophysical Research*, *102*(A8), 17,489–17,497. https://doi.org/10.1029/97JA01182

Dandouras, I., Barthe, A., Penou, E., Brunato, S., Rème, H., Kistler, L. M., et al. (2010). Cluster Ion Spectrometry (CIS) data in the Cluster Active Archive (CAA). In H. Laakso, M. Taylor, & C. Escoubet (Eds.), *The Cluster active archive*, *Astrophysics and Space Science Proceedings* (chap. 3, pp. 51–72). Dordrecht: Springer. https://doi.org/10.1007/978-90-481-3499-1_3

Escoubet, C. P., Fehringer, M., & Goldstein, M. (2001). Introduction: The Cluster mission. *Annales de Geophysique*, *19*(10/12), 1197–1200. https://doi.org/10.5194/angeo-19-1197

Fazakerley, A. N., Lahiff, A. D., Wilson, R. J., Rozum, I., Anekallu, C., West, M., & Bacai, H. (2010). PEACE data in the Cluster active archive. In H. Laakso, M. Taylor, & C. Escoubet (Eds.), *The Cluster active archive*, *Astrophysics and Space Science Proceedings* (chap. 8, pp. 129–144). Dordrecht: Springer. https://doi.org/10.1007/978-90-481-3499-1_8

Fear, R. C., & Milan, S. E. (2012a). The IMF dependence of the local time of transpolar arcs: Implications for formation mechanism. *Journal of Geophysical Research*, *117*, A03213. https://doi.org/10.1029/2011JA017209

Fear, R. C., & Milan, S. E. (2012b). Ionospheric flows relating to transpolar arc formation. *Journal of Geophysical Research*, *117*, A09230. https://doi.org/10.1029/2012JA017830

Fear, R. C., Milan, S. E., Carter, J. A., & Maggiolo, R. (2015). The interaction between transpolar arcs and cusp spots. *Geophysical Research Letters*, *42*, 9685–9693. https://doi.org/10.1002/2015GL066194

Fear, R. C., Milan, S. E., Maggiolo, R., Fazakerley, A. N., Dandouras, I., & Mende, S. B. (2014). Direct observation of closed magnetic flux trapped in the high-latitude magnetosphere. *Science*, *346*(6216), 1506–1510. https://doi.org/10.1126/science.1257377

Frank, L. A., Ackerson, K. L., Paterson, W. R., Lee, J. A., English, M. R., & Pickett, G. L. (1994). The Comprehensive Plasma Instrumentation (CPI) for the Geotail Spacecraft. *Journal of Geomagnetism and Geoelectricity*, *46*(1), 23–37. https://doi.org/10.5636/jgg.46.23

Frank, L. A., Craven, J. D., Burch, J. L., & Winningham, J. D. (1982). Polar views of the Earth's aurora with Dynamics Explorer. *Geophysical Research Letters*, *9*(9), 1001–1004. https://doi.org/10.1029/GL009i009p01001

Frank, L. A., Craven, J. D., Gurnett, D. A., Shawhen, S. D., Burch, J. L., Winningham, J. D., et al. (1986). The theta aurora. *Journal of Geophysical Research*, *91*(A3), 3177–3224. https://doi.org/10.1029/JA091iA03p03177

Frey, H. U., Meade, S. B., Immel, T. J., Fuselier, S. A., Claflin, E. S., Gérard, J.-C., & Hubert, B. (2002). Proton aurora in the cusp. *Journal of Geophysical Research*, *107*(A7), 1091. https://doi.org/10.1029/2001JA900161

Gosling, J. T., Thomsen, M. F., Bame, S. J., Onsager, T., & Russell, C. T. (1990). The electron edge of the low latitude boundary layer during accelerated flow events. *Geophysical Research Letters*, *17*(11), 1833–1836. https://doi.org/10.1029/GL017i011p01833

Greenwald, R. A., Baker, K. B., Dudeney, J. R., Pinnock, M., Jones, T. B., Thomas, E. C., et al. (1995). DARN/SuperDARN: A global view of high-latitude convection. *Space Science Reviews*, *71*(1-4), 761–796. https://doi.org/10.1007/BF00751350

Grocott, A., Badman, S. V., Cowley, S. W. H., Yeoman, T. K., & Cripps, P. J. (2004). The influence of IMF B_Y on the nature of the nightside high-latitude ionospheric flow during intervals of positive IMF B_Z. *Annales de Geophysique*, *22*(5), 1755–1764. https://doi.org/10.5194/angeo-22-1755-2004

Grocott, A., Cowley, S. W. H., & Sigwarth, J. B. (2003). Ionospheric flow during extended intervals of northward but B_Y-dominated IMF. *Annales de Geophysique*, *21*(2), 509–538. https://doi.org/10.5194/angeo-21-509-2003

Grocott, A., Yeoman, T. K., Milan, S. E., & Cowley, S. W. H. (2005). Interhemispheric observations of the ionospheric signature of tail reconnection during IMF-northward non-substorm intervals. *Annales de Geophysique*, *23*, 1763–1770. 1432–0576/ag/2005–23-1763

Gussenhoven, M. S. (1982). Extremely high latitude auroras. *Journal of Geophysical Research*, *87*(A4), 2401–2412. https://doi.org/10.1029/JA087iA04p02401

Heppner, J. P., & Maynard, N. C. (1987). Empirical high-latitude electric field models. *Journal of Geophysical Research*, *92*(A5), 4467–4489. https://doi.org/10.1029/JA092iA05p04467

Johnstone, A. D., Alsop, C., Burge, S., Carter, P. J., Coates, A. J., Coker, A. J., et al. (1997). PEACE: A plasma electron and current experiment. *Space Science Reviews*, *79*(1/2), 351–398. https://doi.org/10.1023/A:1004938001388

Kokubun, S., Yamamoto, T., Acuña, M., Hayashi, K., Shiokawa, K., & Kawano, H. (1994). The Geotail magnetic field experiment. *Journal of Geomagnetism and Geoelectricity*, *46*(1), 7–21. https://doi.org/10.5636/jgg.46.7

Kullen, A. (2000). The connection between transpolar arcs and magnetotail rotation. *Geophysical Research Letters*, *27*(1), 73–76. https://doi.org/10.1029/1999GL010675

Kullen, A., Brittnacher, M., Cumnock, J. A., & Blomberg, L. G. (2002). Solar wind dependence of the occurrence and motion of polar auroral arcs: A statistical study. *Journal of Geophysical Research*, *107*(A11), 1362. https://doi.org/10.1029/2002JA009245

Kullen, A., Fear, R. C., Milan, S. E., Carter, J. A., & Karlsson, T. (2015). The statistical difference between bending arcs and regular polar arcs. *Journal of Geophysical Research: Space Physics*, *120*, 10,443–10,465. https://doi.org/10.1002/2015JA021298

Kullen, A., & Janhunen, P. (2004). Relation of polar auroral arcs to magnetotail twisting and IMF rotation: A systematic MHD simulation study. *Annales de Geophysique*, *22*(3), 951–970. https://doi.org/10.5194/angeo-22-951-2004

Mailyan, B., Shi, Q. -Q., Kullen, A., Maggiolo, R., Zhang, Y., Fear, R. C., et al. (2015). Transpolar arc observation after solar wind entry into the high-latitude magnetosphere. *Journal of Geophysical Research: Space Physics*, *120*, 3525–3534. https://doi.org/10.1002/2014JA020912

Makita, K., Meng, C.-I., & Akasofu, S.-I. (1991). Transpolar auroras, their particle precipitation, and IMF B_y component. *Journal of Geophysical Research*, *96*(A8), 14,085–14,095. https://doi.org/10.1029/90JA02323

Mende, S. B., Heetderks, H., Frey, H. U., Lampton, M., Geller, S. P., Abiad, R., et al. (2000). Far ultraviolet imaging from the IMAGE spacecraft: 2. Wideband FUV imaging. *Space Science Reviews*, *91*(1/2), 271–285. https://doi.org/10.1023/A:1005227915363

Mende, S. B., Heetderks, H., Frey, H. U., Lampton, M., Geller, S. P., Habraken, S., et al. (2000). Far ultraviolet imaging from the IMAGE spacecraft: 1. System design. *Space Science Reviews*, *91*(1/2), 243–270. https://doi.org/10.1023/A:1005271728567

Mende, S. B., Heetderks, H., Frey, H. U., Stock, J. M., Lampton, M., Geller, S. P., et al. (2000). Far ultraviolet imaging from the IMAGE spacecraft: 3. Spectral imaging of Lyman-α and OI 135.6 nm. *Space Science Reviews*, *91*(1/2), 287–318. https://doi.org/10.1023/A:1005292301251

Milan, S. E., Hubert, B., & Grocott, A. (2005). Formation and motion of a transpolar arc in response to dayside and nightside reconnection. *Journal of Geophysical Research*, *110*, A01212. https://doi.org/10.1029/2004JA010835

Newell, P. T., Meng, C.-I., Sibeck, D. G., & Lepping, R. (1989). Some low-altitude cusp dependencies on the interplanetary magnetic field. *Journal of Geophysical Research*, *94*(A7), 8921–8927. https://doi.org/10.1029/JA094iA07p08921

Øieroset, M., Phan, T. D., Gosling, J. T., Fujimoto, M., & Angelopoulos, V. (2015). Electron and ion edges and the associated magnetic topology of the reconnecting magnetopause. *Journal of Geophysical Research: Space Physics*, *120*, 9294–9306. https://doi.org/10.1002/2015JA021580

Peterson, W. K., & Shelley, E. G. (1984). Origin of the plasma in a cross polar cap auroral feature (theta aurora). *Journal of Geophysical Research*, *89*(A8), 6729–6736. https://doi.org/10.1029/JA089iA08p06729

Pitout, F., Escoubet, C. P., Klecker, B., & Rème, H. (2006). Cluster survey of the mid-altitude cusp: 1. Size, location, and dynamics. *Annales de Geophysique*, *24*(11), 3011–3026. https://doi.org/10.5194/angeo-24-3011-2006

Rème, H., Aoustin, C., Bosqued, J. M., Dandouras, I., Lavraud, B., Sauvaud, J. A., et al. (2001). First multispacecraft ion measurements in and near the Earth's magnetosphere with the identical Cluster ion spectrometry (CIS) experiment. *Annales Geophysicae*, *19*, 1303–1354. https://doi.org/10.5194/angeo-19-1303-2001

Ruohoniemi, J. M., & Baker, K. B. (1998). Large-scale imaging of high-latitude convection with super dual auroral radar network HF radar observations. *Journal of Geophysical Research*, *103*(A9), 20,797–20,811. https://doi.org/10.1029/98JA01288

Ruohoniemi, J. M., & Greenwald, R. A. (1996). Statistical patterns of high-latitude convection obtained from Goose Bay HF radar observations. *Journal of Geophysical Research*, *101*(A10), 21,743–21,763. https://doi.org/10.1029/96JA01584

Shue, J.-H., Song, P., Russell, C. T., Steinberg, J. T., Chao, J. K., Zastenker, G., et al. (1998). Magnetopause location under extreme solar wind conditions. *Journal of Geophysical Research*, *103*(A8), 17,691–17,700. https://doi.org/10.1029/98JA01103

Siscoe, G. L., & Huang, T. S. (1985). Polar cap inflation and deflation. *Journal of Geophysical Research*, *90*(A1), 543–547. https://doi.org/10.1029/JA090iA01p00543

Tsyganenko, N. A. (1989). A magnetospheric magnetic field model with a warped tail current sheet. *Planetary and Space Science*, *37*(1), 5–20. https://doi.org/10.1016/0032-0633(89)90066-4

Tsyganenko, N. A. (1995). Modeling the Earth's magnetospheric magnetic field confined within a realistic magnetopause. *Journal of Geophysical Research*, *100*(A4), 5599–5612. https://doi.org/10.1029/94JA03193

Tsyganenko, N. A. (2002). A model of the near magnetosphere magnetic field. 2. Parameterization and fitting to observations. *Journal of Geophysical Research*, *107*(A8), 1176. https://doi.org/10.1029/2001JA000220

Valladares, C. E., Carlson, H. C., & Fukui, K. (1994). Interplanetary magnetic field dependency of stable Sun-aligned polar cap arcs. *Journal of Geophysical Research*, *99*(A4), 6247–6272. https://doi.org/10.1029/93JA03255

Zhu, L., Schunk, R. W., & Sojka, J. J. (1997). Polar cap arcs: A review. *Journal of Atmospheric and Terrestrial Physics*, *59*(10), 1087–1126. https://doi.org/10.1016/S1364-6826(96)00113-7

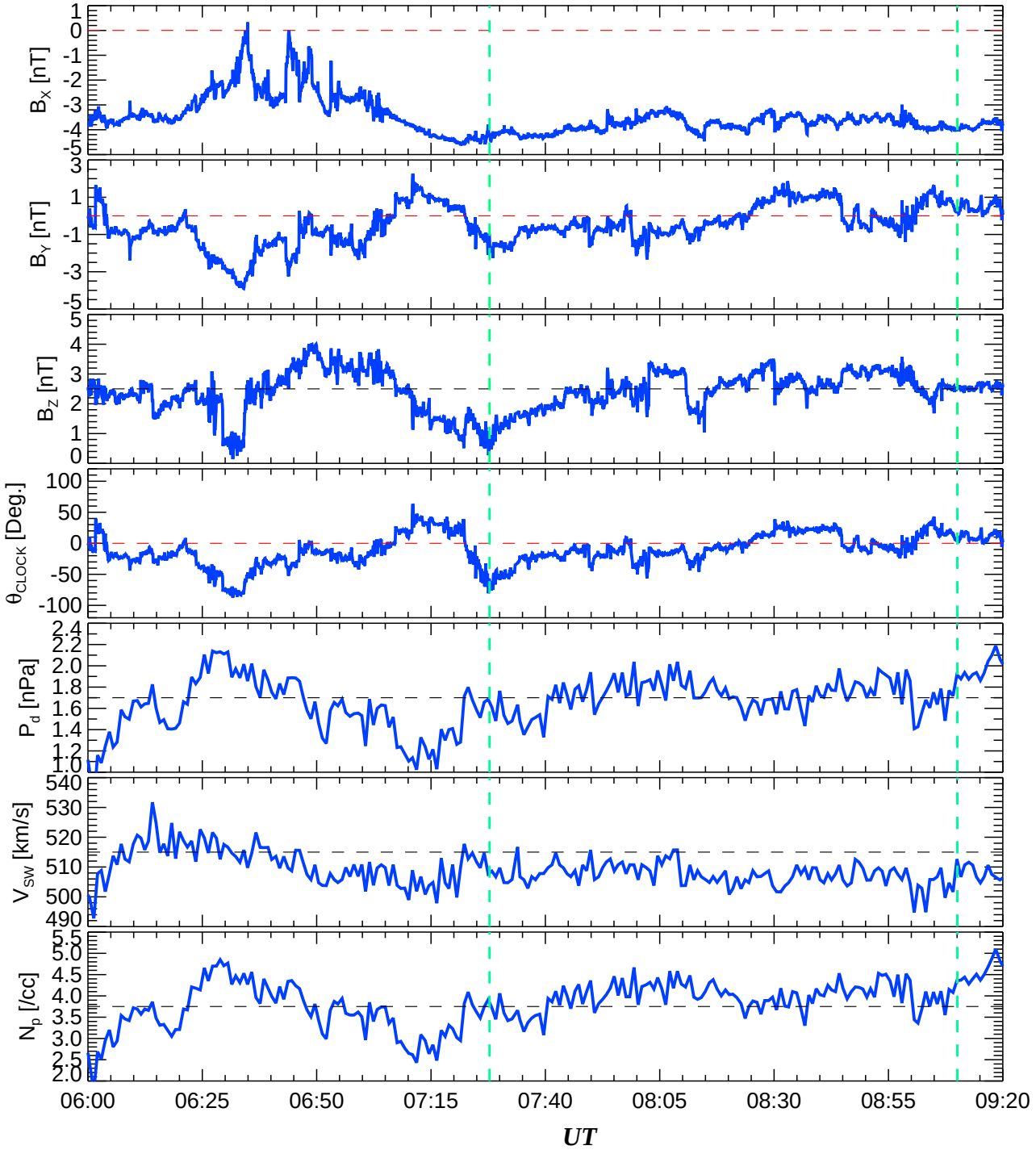
B_X [nT]
B_Y [nT]
B_Z [nT]
θ_CLOCK [Deg.]
P_d [nPa]
V_SW [km/s]
N_p [/cc]
06:00
06:25
06:50
07:15
07:40
08:05
08:30
08:55
09:20
UT

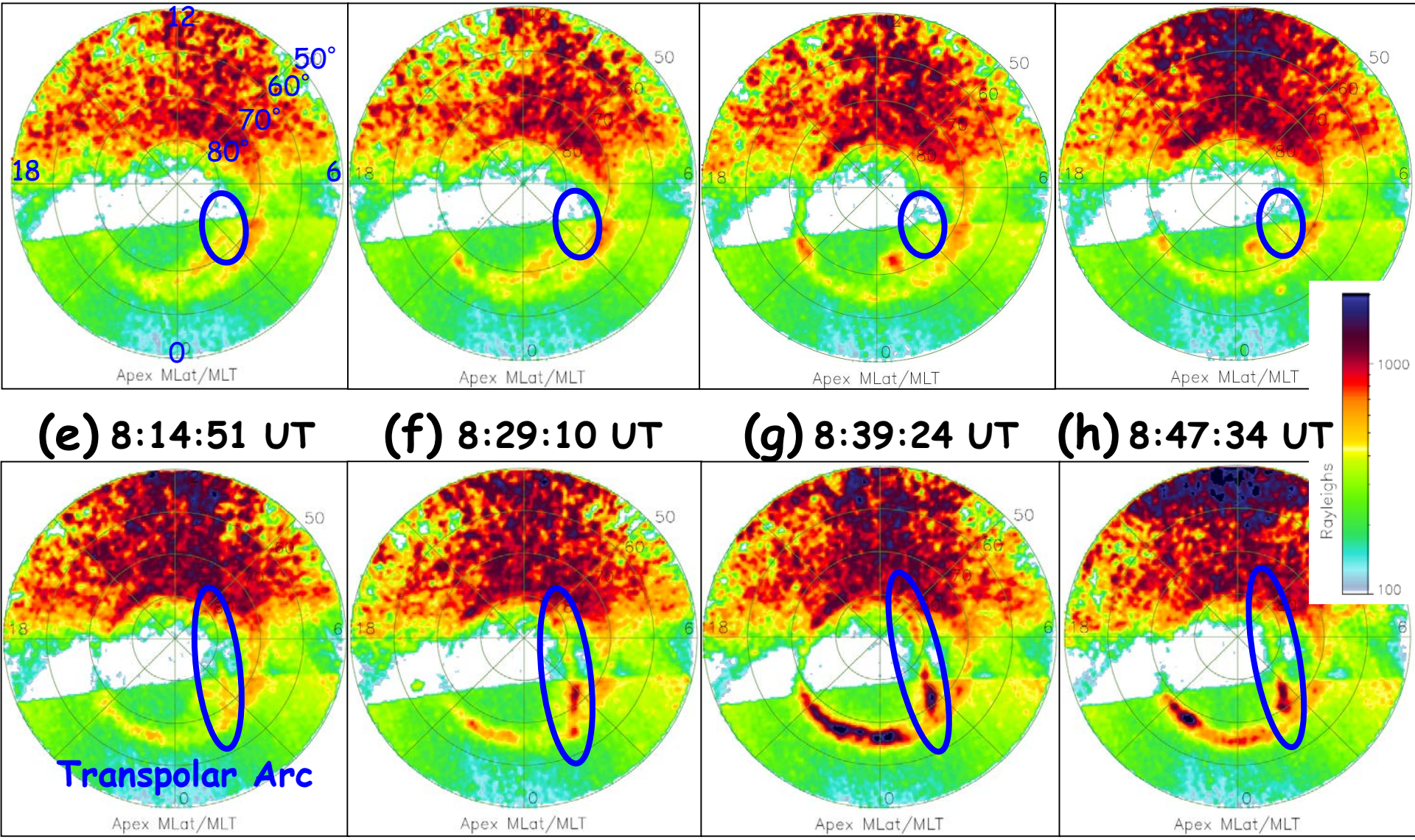
(a) 7:27:48 UT
(b) 7:35:59 UT
(c) 7:46:12 UT
(d) 7:58:29 UT
(e) 8:14:51 UT
(f) 8:29:10 UT
(g) 8:39:24 UT
(h) 8:47:34 UT
12
18
6
0
50°
60°
70°
80°
Apex MLat/MLT
Transpolar Arc
Rayleighs
1000
100

(i) 8:51:40 UT (j) 8:55:45 UT (k) 9:03:56 UT (l) 9:10:04UT

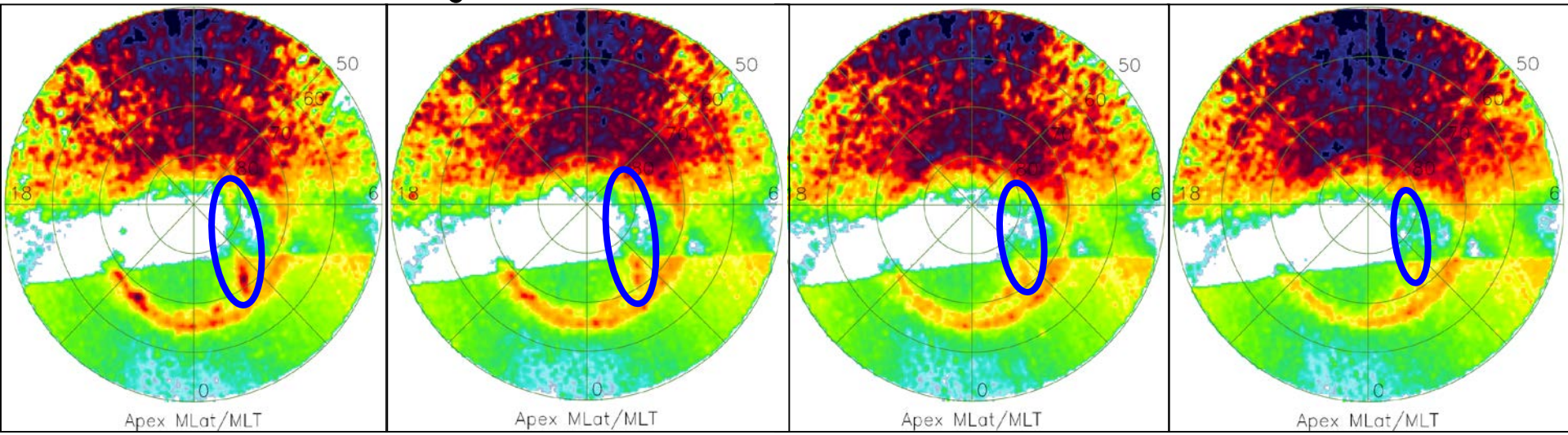

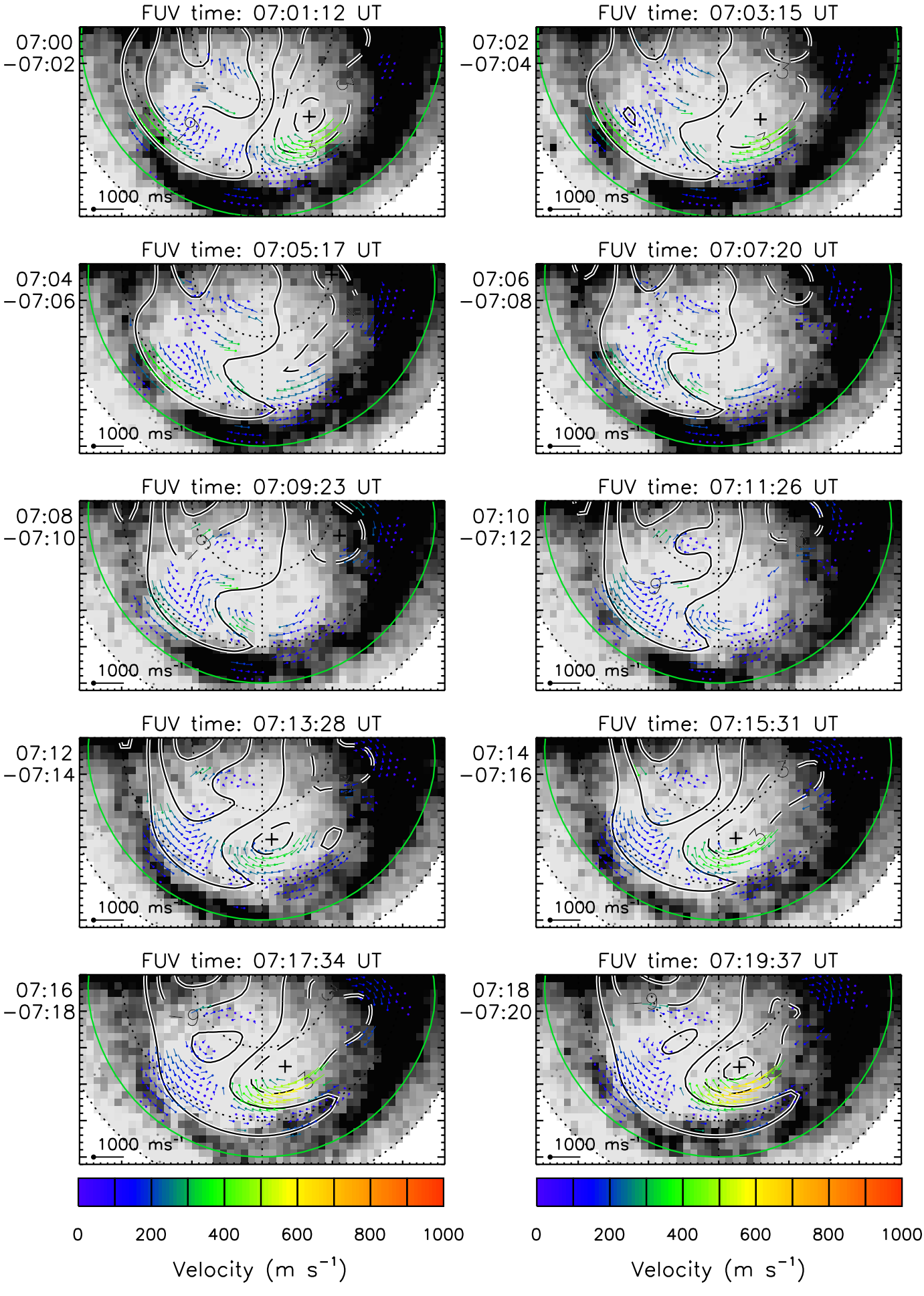
FUV time: 07:01:12 UT
07:00
−07:02
1000 ms⁻¹
FUV time: 07:03:15 UT
07:02
−07:04
1000 ms⁻¹
FUV time: 07:05:17 UT
07:04
−07:06
1000 ms⁻¹
FUV time: 07:07:20 UT
07:06
−07:08
1000 ms⁻¹
FUV time: 07:09:23 UT
07:08
−07:10
1000 ms⁻¹
FUV time: 07:11:26 UT
07:10
−07:12
1000 ms⁻¹
FUV time: 07:13:28 UT
07:12
−07:14
1000 ms⁻¹
FUV time: 07:15:31 UT
07:14
−07:16
1000 ms⁻¹
FUV time: 07:17:34 UT
07:16
−07:18
1000 ms⁻¹
FUV time: 07:19:37 UT
07:18
−07:20
1000 ms⁻¹
0
200
400
600
800
1000
Velocity (m s⁻¹)
0
200
400
600
800
1000
Velocity (m s⁻¹)

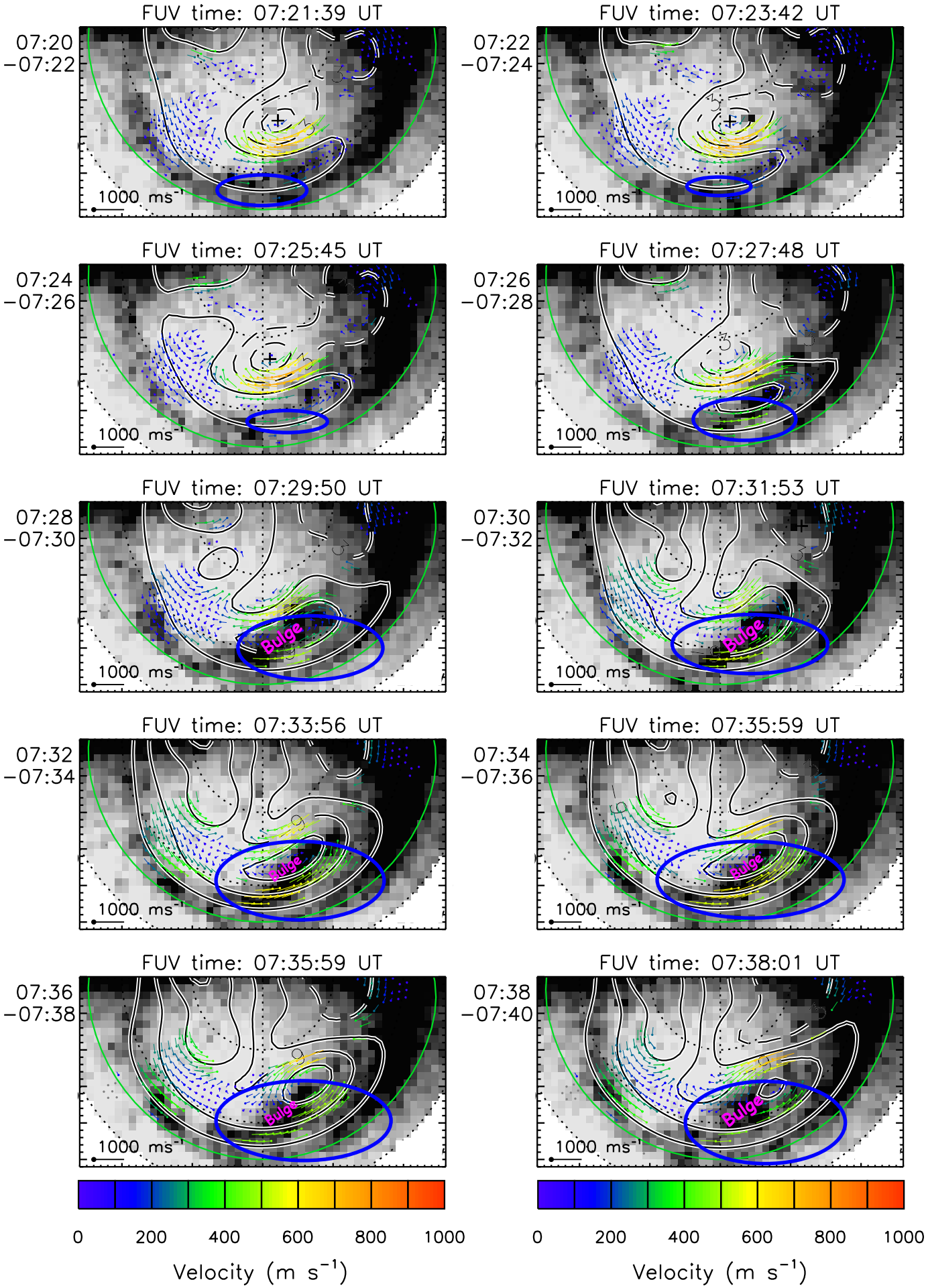
FUV time: 07:21:39 UT
07:20
−07:22
1000 ms⁻¹
FUV time: 07:23:42 UT
07:22
−07:24
1000 ms⁻¹
FUV time: 07:25:45 UT
07:24
−07:26
1000 ms⁻¹
FUV time: 07:27:48 UT
07:26
−07:28
1000 ms⁻¹
FUV time: 07:29:50 UT
07:28
−07:30
Bulge
1000 ms⁻¹
FUV time: 07:31:53 UT
07:30
−07:32
Bulge
1000 ms⁻¹
FUV time: 07:33:56 UT
07:32
−07:34
Bulge
1000 ms⁻¹
FUV time: 07:35:59 UT
07:34
−07:36
Bulge
1000 ms⁻¹
FUV time: 07:35:59 UT
07:36
−07:38
Bulge
1000 ms⁻¹
FUV time: 07:38:01 UT
07:38
−07:40
Bulge
1000 ms⁻¹
0
200
400
600
800
1000
Velocity (m s⁻¹)
0
200
400
600
800
1000
Velocity (m s⁻¹)

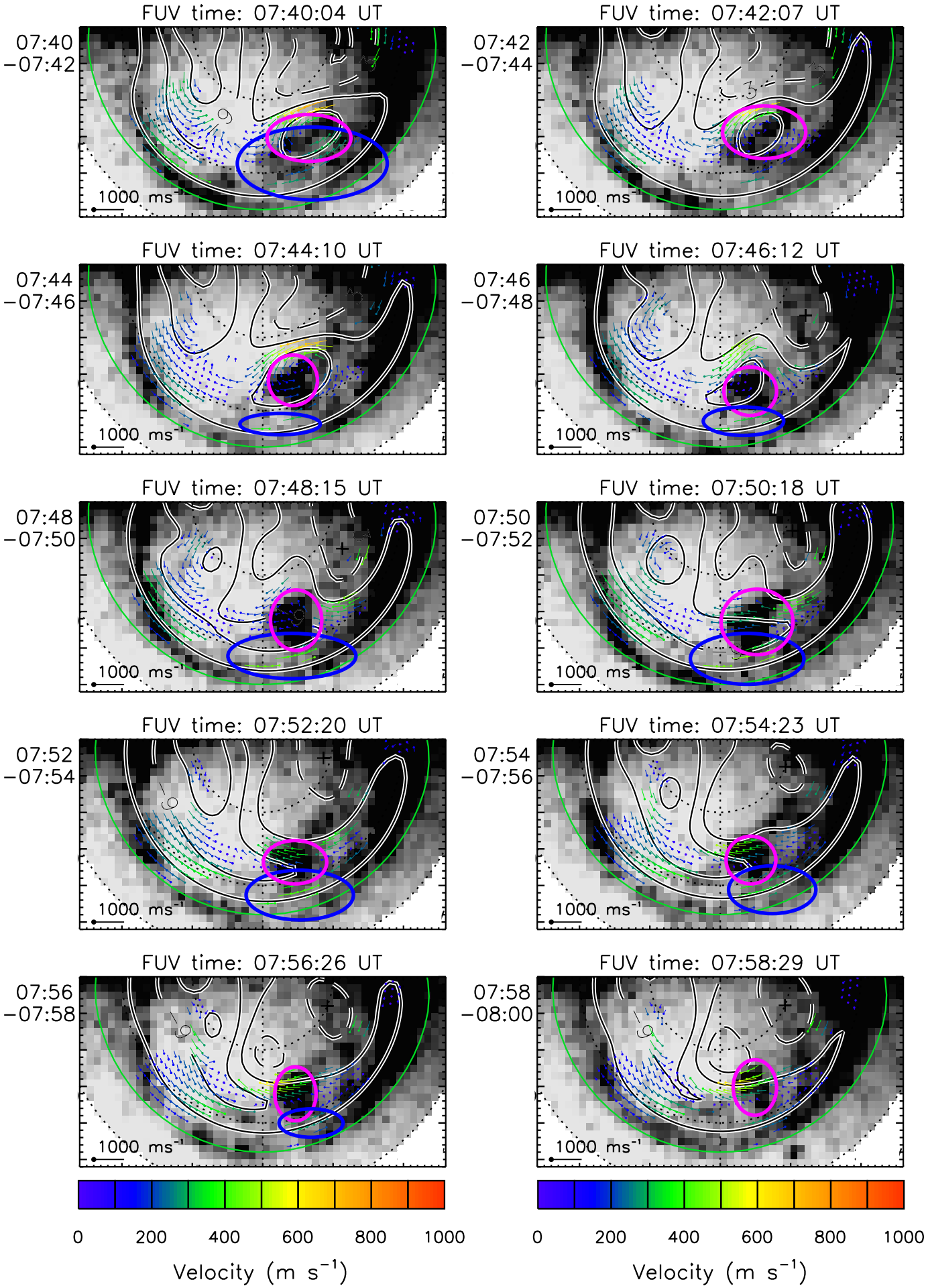
FUV time: 07:40:04 UT
07:40
−07:42
1000 ms⁻¹
FUV time: 07:42:07 UT
07:42
−07:44
1000 ms⁻¹
FUV time: 07:44:10 UT
07:44
−07:46
1000 ms⁻¹
FUV time: 07:46:12 UT
07:46
−07:48
1000 ms⁻¹
FUV time: 07:48:15 UT
07:48
−07:50
1000 ms⁻¹
FUV time: 07:50:18 UT
07:50
−07:52
1000 ms⁻¹
FUV time: 07:52:20 UT
07:52
−07:54
1000 ms⁻¹
FUV time: 07:54:23 UT
07:54
−07:56
1000 ms⁻¹
FUV time: 07:56:26 UT
07:56
−07:58
1000 ms⁻¹
FUV time: 07:58:29 UT
07:58
−08:00
1000 ms⁻¹
0
200
400
600
800
1000
Velocity (m s⁻¹)
0
200
400
600
800
1000
Velocity (m s⁻¹)

7:27:48 UT (TPA Onset)

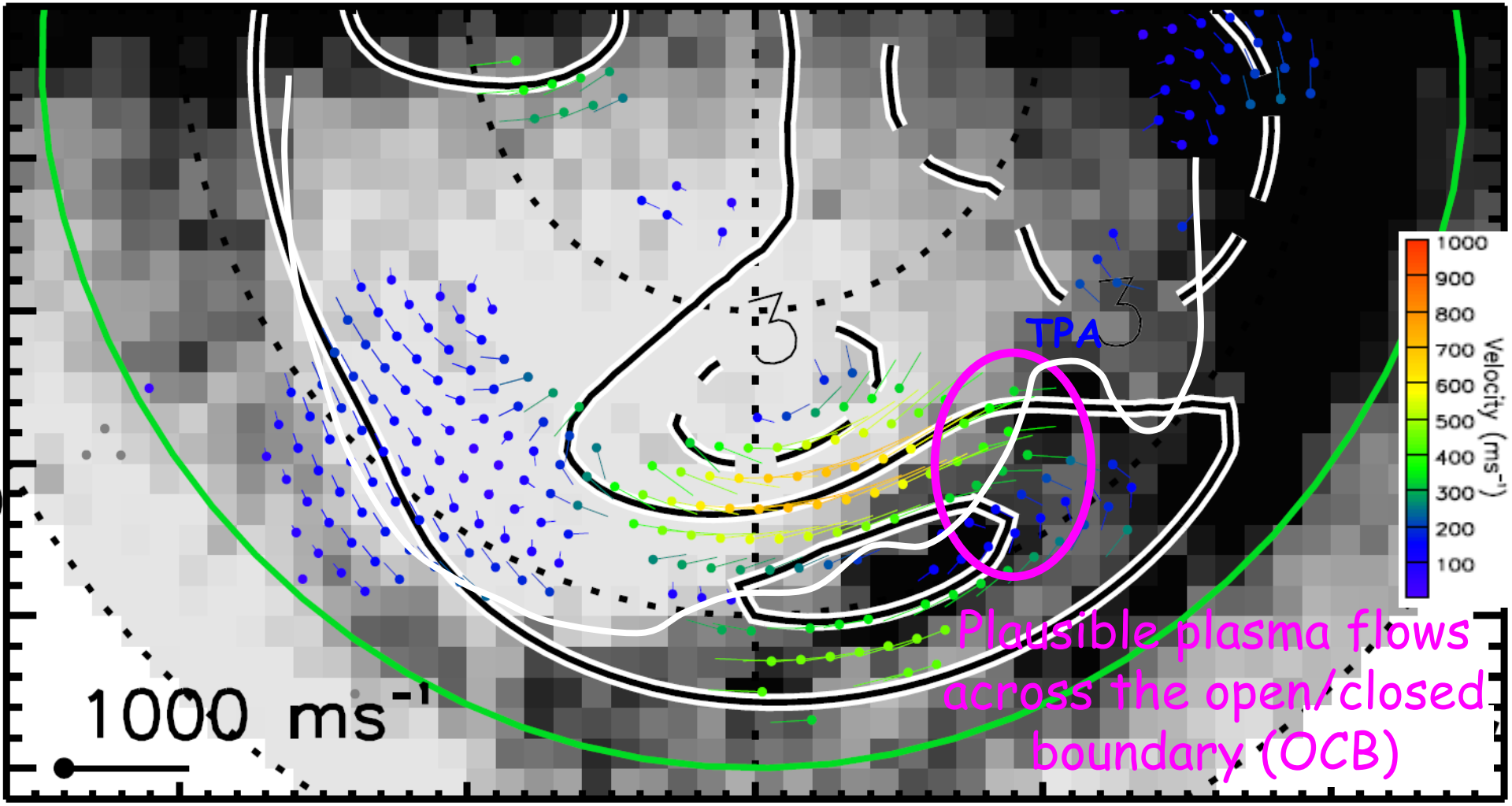

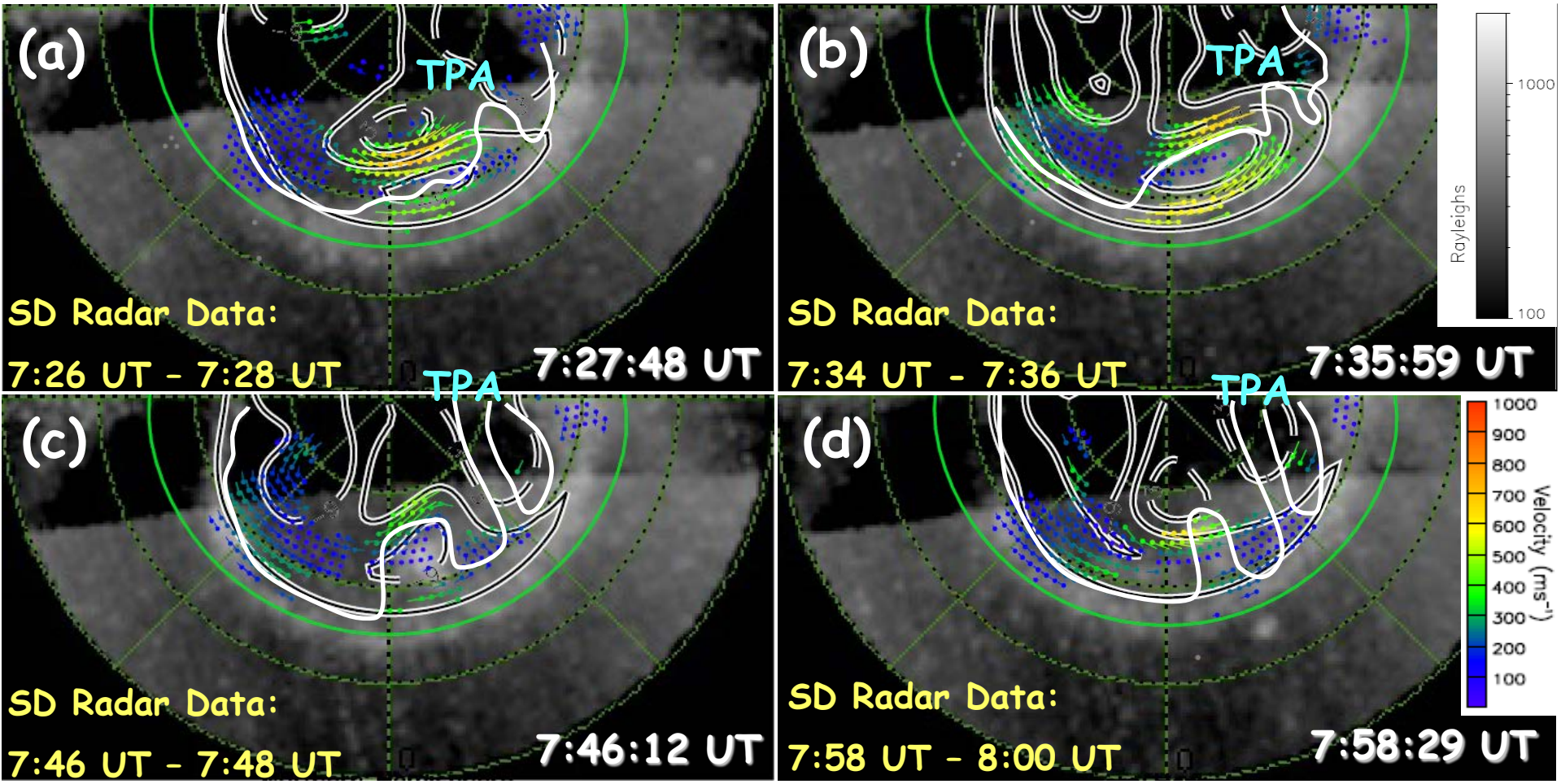
(a)
TPA
SD Radar Data:
7:26 UT – 7:28 UT
7:27:48 UT
(b)
TPA
SD Radar Data:
7:34 UT – 7:36 UT
7:35:59 UT
Rayleighs
1000
100
(c)
TPA
SD Radar Data:
7:46 UT – 7:48 UT
7:46:12 UT
(d)
TPA
SD Radar Data:
7:58 UT – 8:00 UT
7:58:29 UT
1000
900
800
700
600
500
400
300
200
100
Velocity (ms⁻¹)

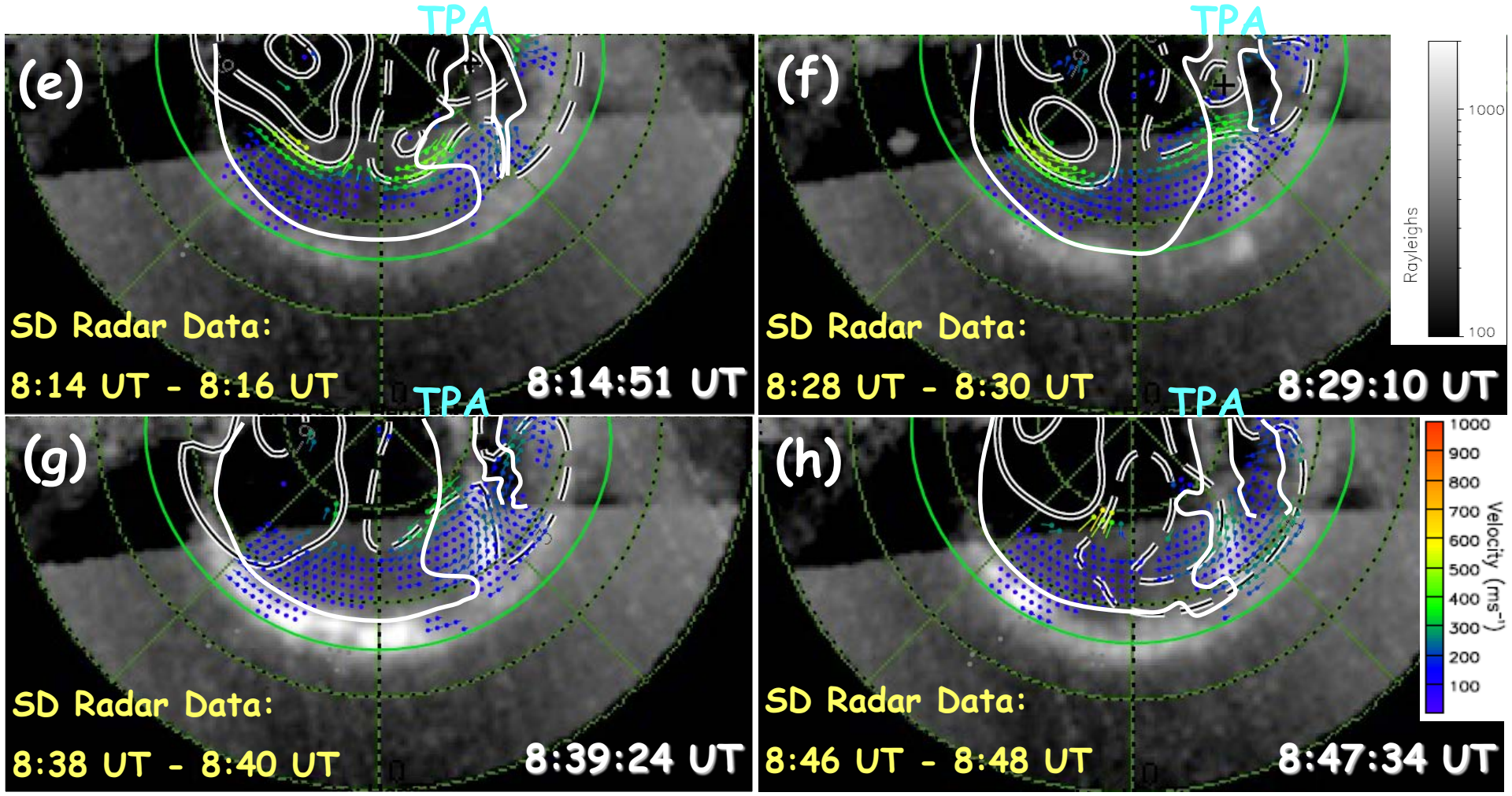
(e)
TPA
SD Radar Data:
8:14 UT - 8:16 UT
8:14:51 UT
(f)
TPA
SD Radar Data:
8:28 UT - 8:30 UT
8:29:10 UT
Rayleighs
1000
100
(g)
TPA
SD Radar Data:
8:38 UT - 8:40 UT
8:39:24 UT
(h)
TPA
SD Radar Data:
8:46 UT - 8:48 UT
8:47:34 UT
Velocity (ms⁻¹)
1000
900
800
700
600
500
400
300
200
100

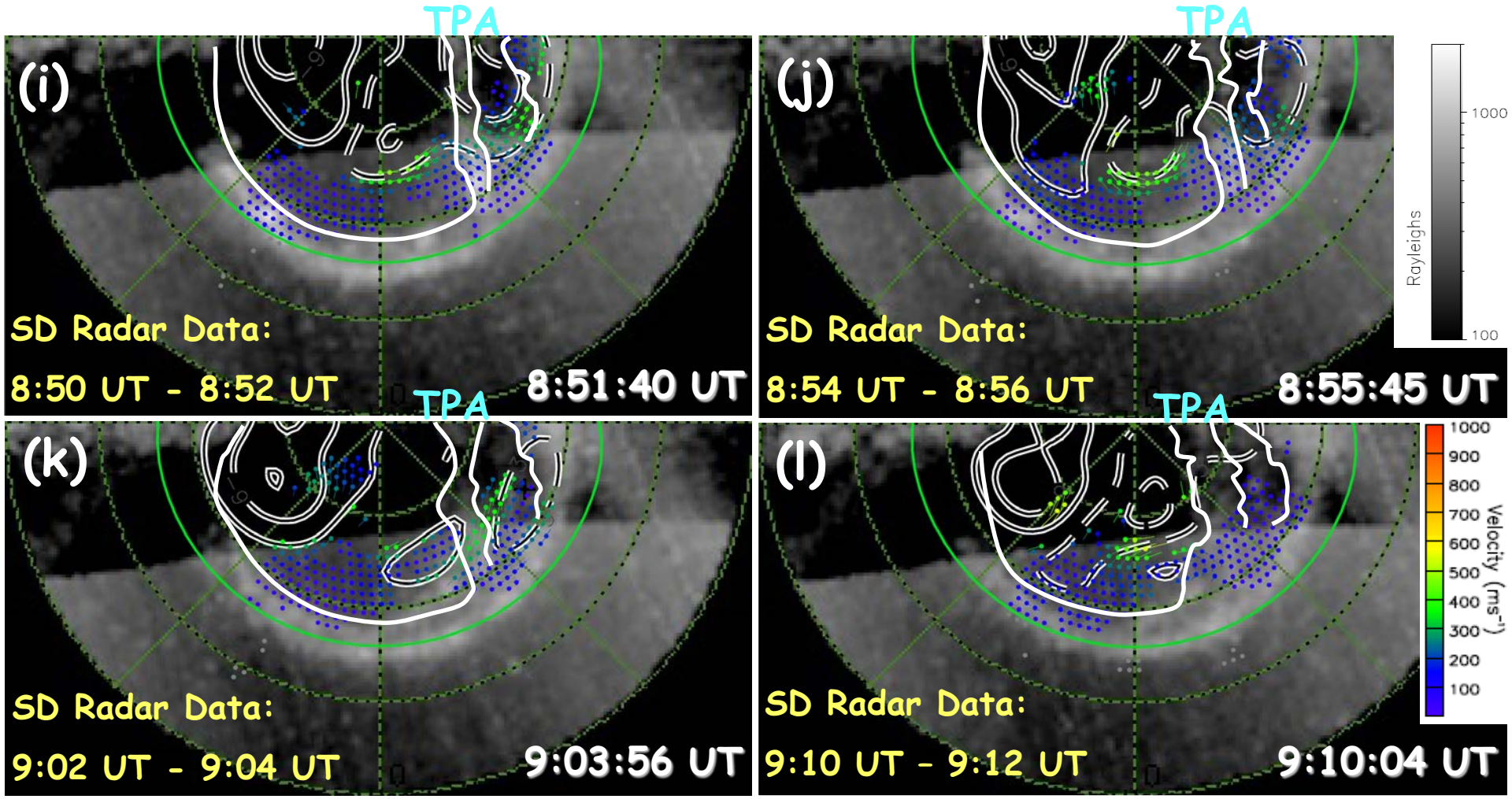
(i)
TPA
SD Radar Data:
8:50 UT - 8:52 UT
8:51:40 UT
(j)
TPA
SD Radar Data:
8:54 UT - 8:56 UT
8:55:45 UT
Rayleighs
1000
100
(k)
TPA
SD Radar Data:
9:02 UT - 9:04 UT
9:03:56 UT
(l)
TPA
SD Radar Data:
9:10 UT - 9:12 UT
9:10:04 UT
1000
900
800
700
600
500
400
300
200
100
Velocity (ms⁻¹)

IMF- $B_z > 0$ AND IMF-$B_y < 0$

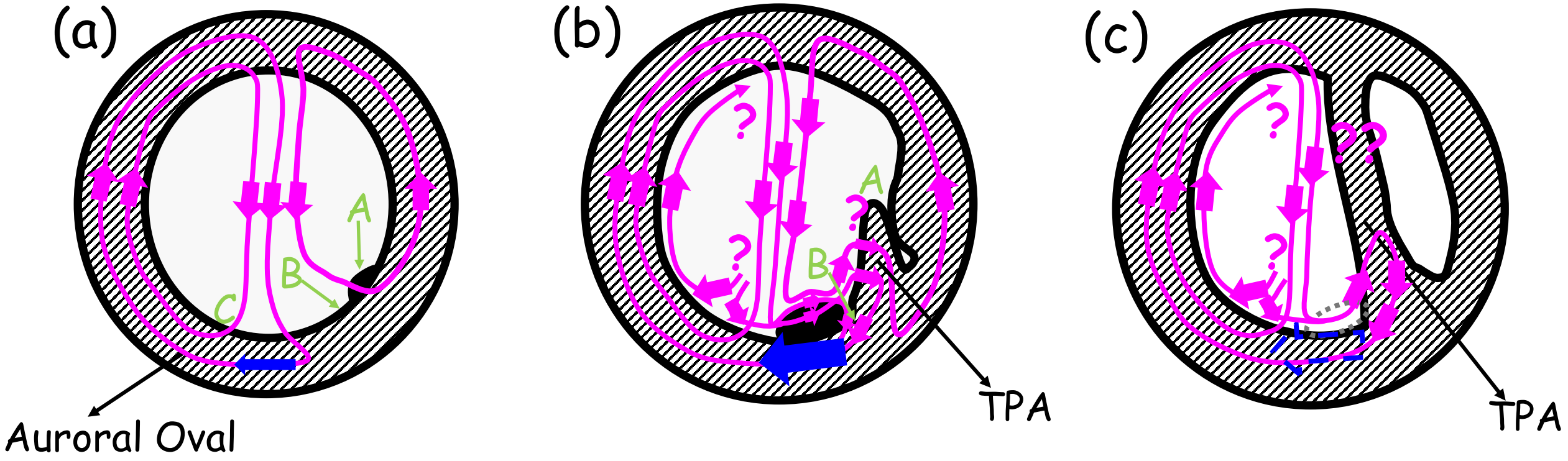

TRINNI Flows (weak)

TRINNI Flows

No TRINNI Flows

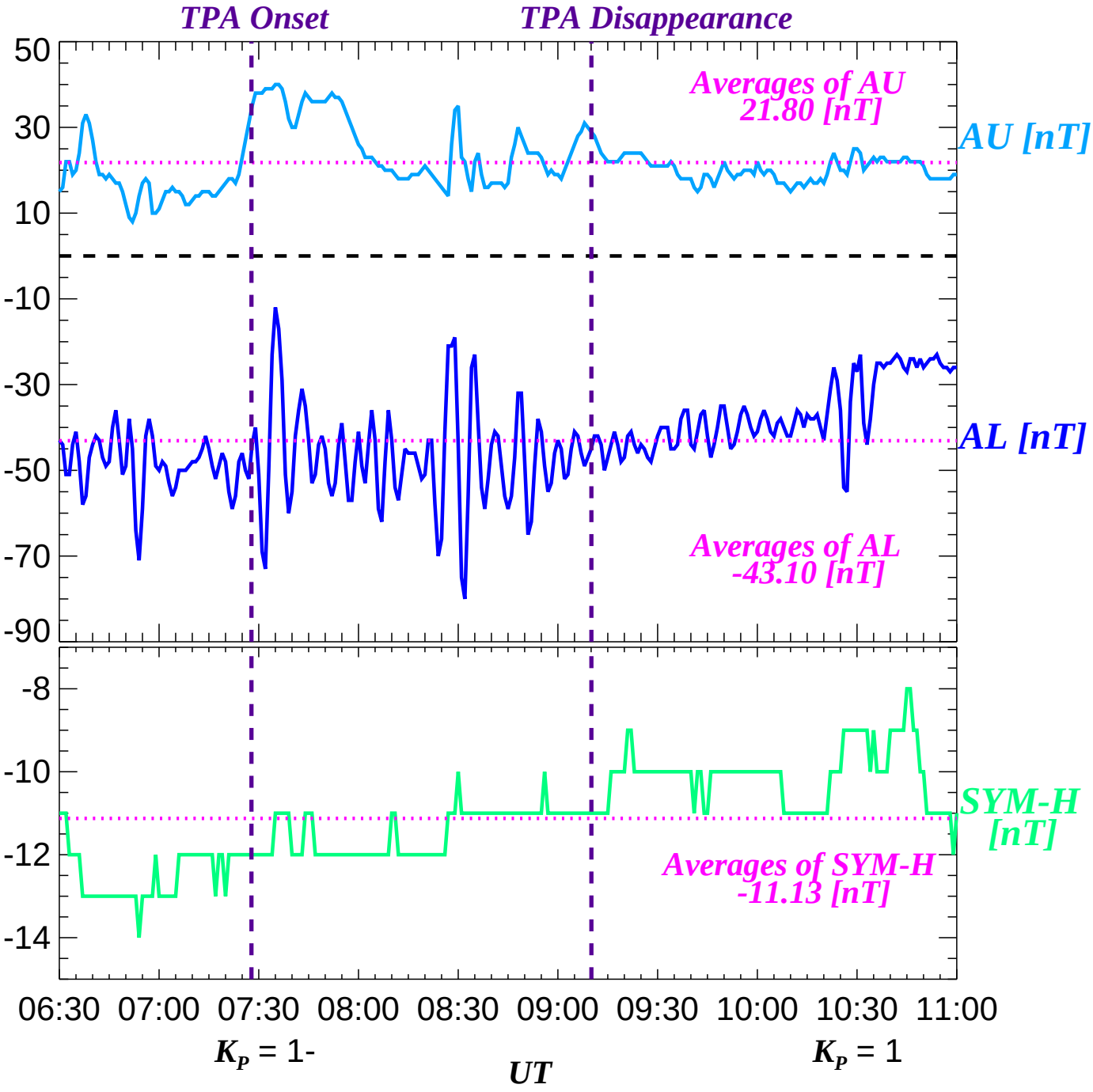
TPA Onset
TPA Disappearance
Averages of AU
21.80 [nT]
AU [nT]
Averages of AL
-43.10 [nT]
AL [nT]
Averages of SYM-H
-11.13 [nT]
SYM-H
[nT]
50
30
10
-10
-30
-50
-70
-90
-8
-10
-12
-14
06:30
07:00
07:30
08:00
08:30
09:00
09:30
10:00
10:30
11:00
K_P = 1-
K_P = 1
UT

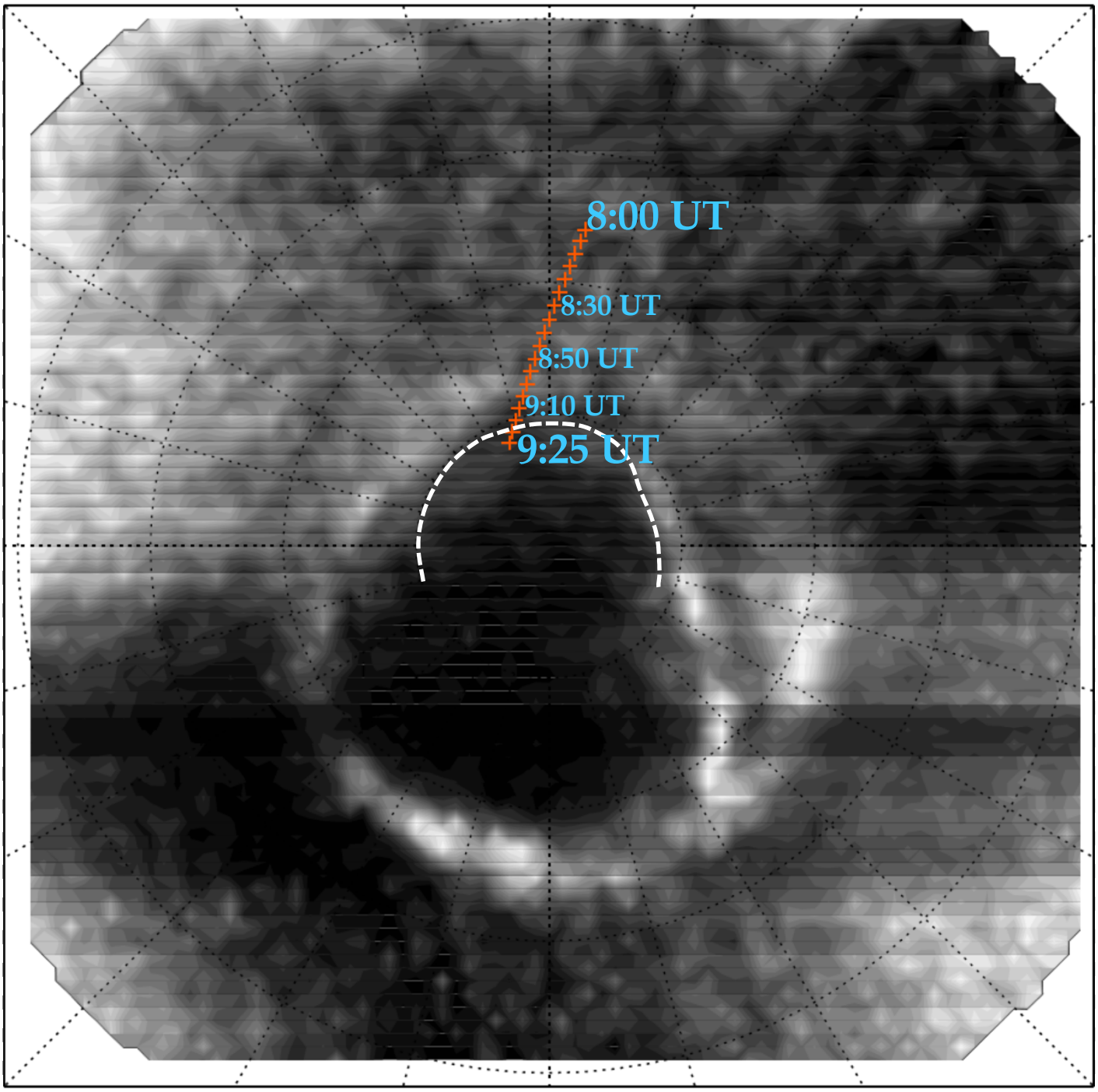
8:00 UT
8:30 UT
8:50 UT
9:10 UT
9:25 UT

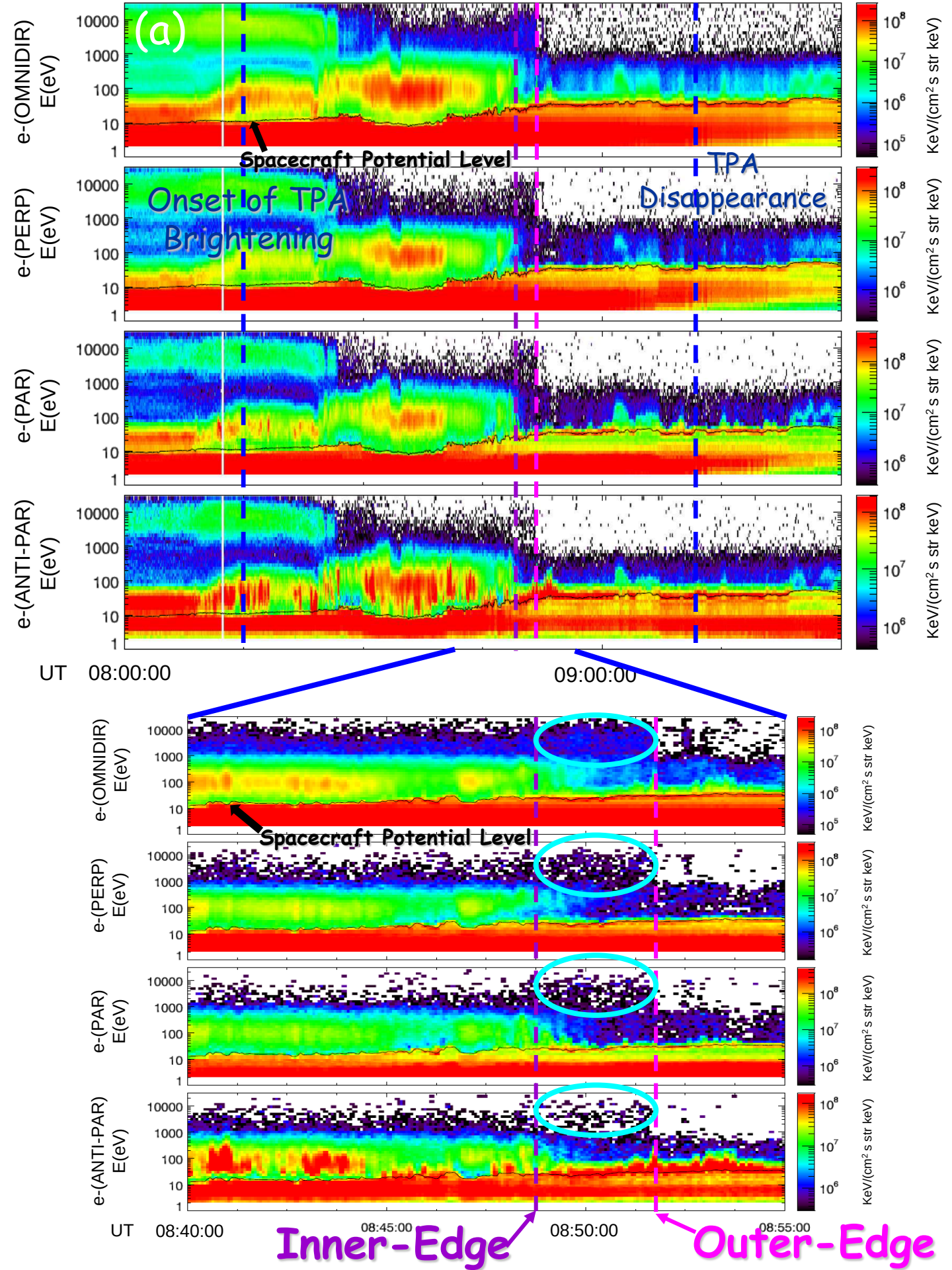
(a)
e-(OMNIDIR) E(eV)
e-(PERP) E(eV)
e-(PAR) E(eV)
e-(ANTI-PAR) E(eV)
10000
1000
100
10
1
Spacecraft Potential Level
Onset of TPA Brightening
TPA Disappearance
KeV/(cm² s str keV)
UT 08:00:00
09:00:00
08:40:00
08:45:00
08:50:00
08:55:00
Inner-Edge
Outer-Edge

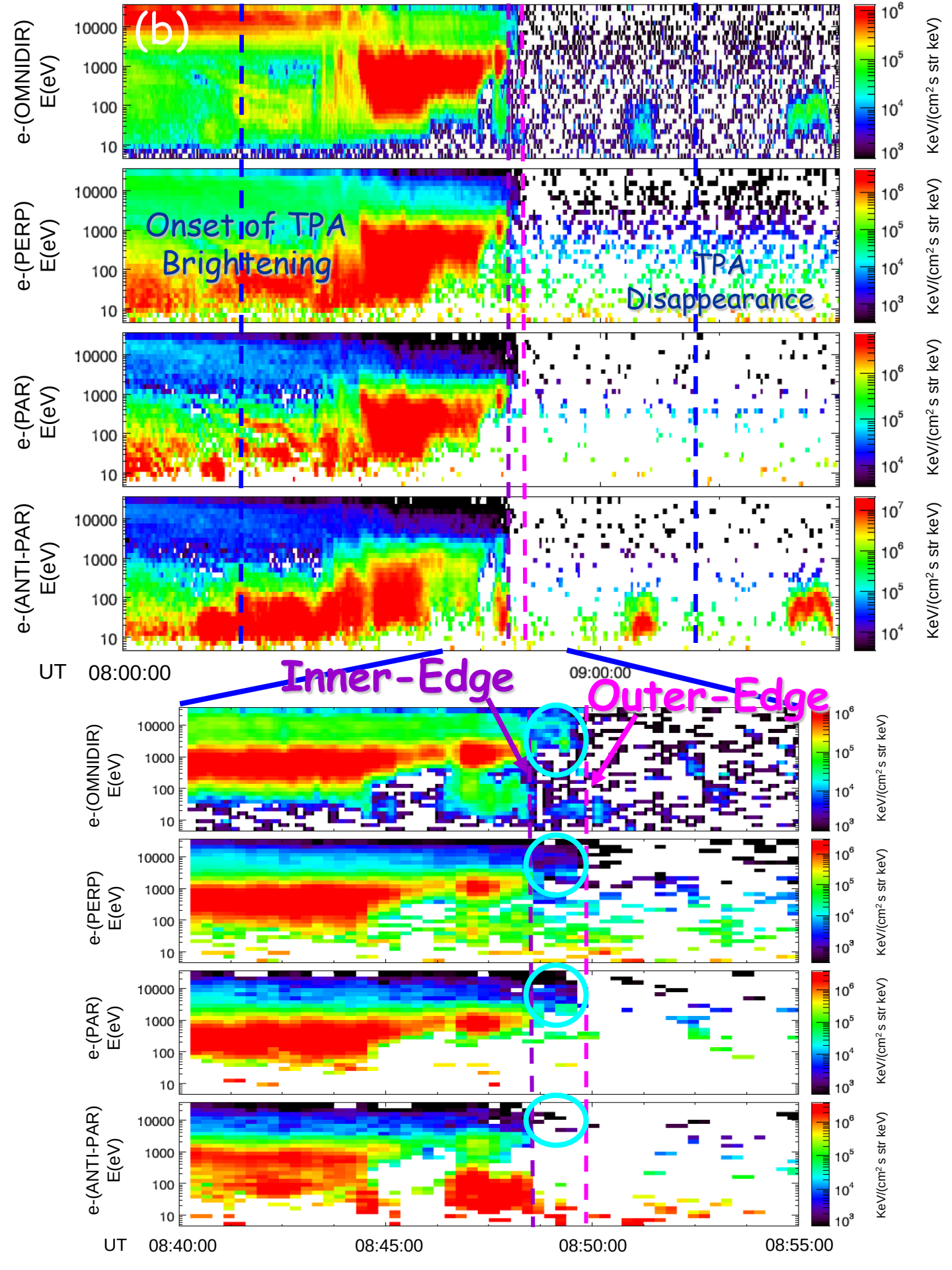
(b)
e-(OMNIDIR) E(eV)
e-(PERP) E(eV)
e-(PAR) E(eV)
e-(ANTI-PAR) E(eV)
10000
1000
100
10
KeV/(cm² s str keV)
Onset of TPA Brightening
TPA Disappearance
UT 08:00:00
09:00:00
Inner-Edge
Outer-Edge
UT 08:40:00
08:45:00
08:50:00
08:55:00

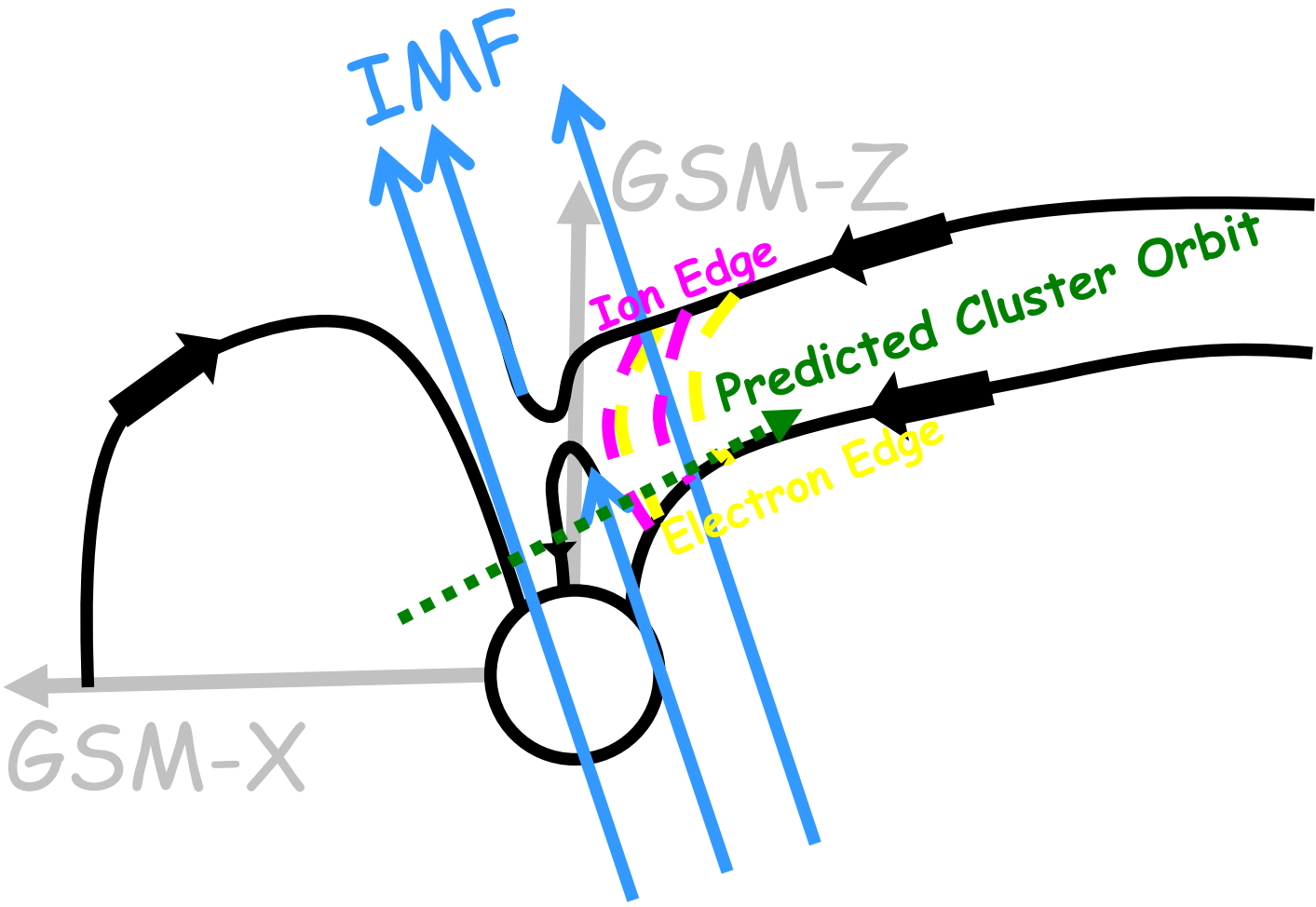
IMF
GSM-Z
Ion Edge
Predicted Cluster Orbit
Electron Edge
GSM-X

Journal of Geophysical Research -Space Physics-

Supporting Information for

Subsidence of Ionospheric Flows Triggered by Magnetotail Magnetic Reconnection During Transpolar Arc Brightening

Motoharu Nowada[1], Robert C. Fear[2], Adrian Grocott[3], Quan-Qi Shi[1], Jun Yang[1], Qiu-Gang Zong[4], Yong Wei[5], Sui-Yan Fu[4], Zu-Yin Pu[4], Bagrat Mailyan[1], and Hui Zhang[6]

1: Center for Space Weather Sciences, Institute of Space Science, School of Space Science and Physics, Shandong University at Weihai, Shandong, People Republic of China.

2: Department of Physics and Astronomy, University of Southampton, Southampton, United Kingdom.

3: Space and Planetary Physics Group, Department of Physics, Lancaster University, Lancaster, United Kingdom.

4: Institute of Space Physics and Applied Technology, School of Earth and Space Sciences, Peking University, Beijing, People Republic of China.

5: Key Laboratory of Earth and Planetary Physics, Institute of Geology and Geophysics, Chinese Academy of Sciences, Beijing, People Republic of China.

6: Geophysical Institute, University of Alaska, Fairbanks, U.S.

Contents of this file

Introduction

The overlaid plots of the SuperDARN backscatter and the auroral image data obtained with Wideband Imaging Camera (WIC) in the Far Ultraviolet (FUV) instrument onboard the IMAGE satellite during about 1.1 hours between 8:00 UT and 9:10 UT are provided. This interval includes the "TPA growth" (until 8:12:48 UT) and "TPA brightening" (from 8:14:51 UT to 9:10:04 UT) stages in figure. Furthermore, the full set of the aurora image data obtained with the FUV-WIC of IMAGE during 2 hours between 7:20 UT (7:19:37 UT) and 9:20 UT (9:20:18 UT) is displayed in the movie (ms01). The auroral imager snapshots for 2 hours clearly show the main theta auroral oval, and the processes of the TPA growth and the complete connection to the dayside region.

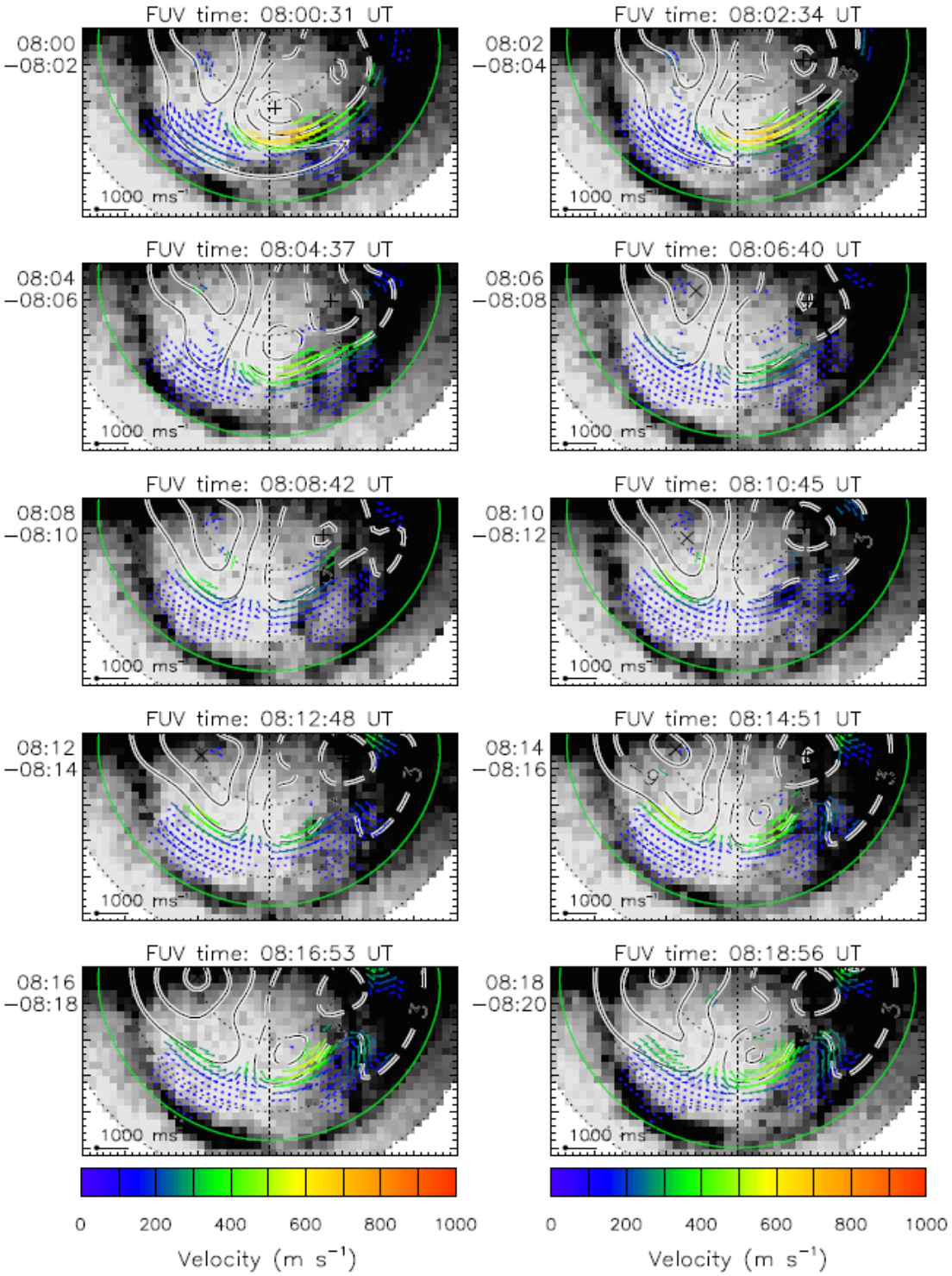

Figure S1(a). The nightside ionospheric flow streamlines and their line-of-sight velocity vectors measured by SuperDARN radars in the northern hemisphere, overlaid by the FUV-WIC data from IMAGE, are shown during 1.1 hours between 8:00 UT and 9:10 UT, when the TPA was growing (until 8:12:48 UT) and brightening (from 8:14:51 UT to 9:10:04 UT). Figure format is the same as that in Figure 3.

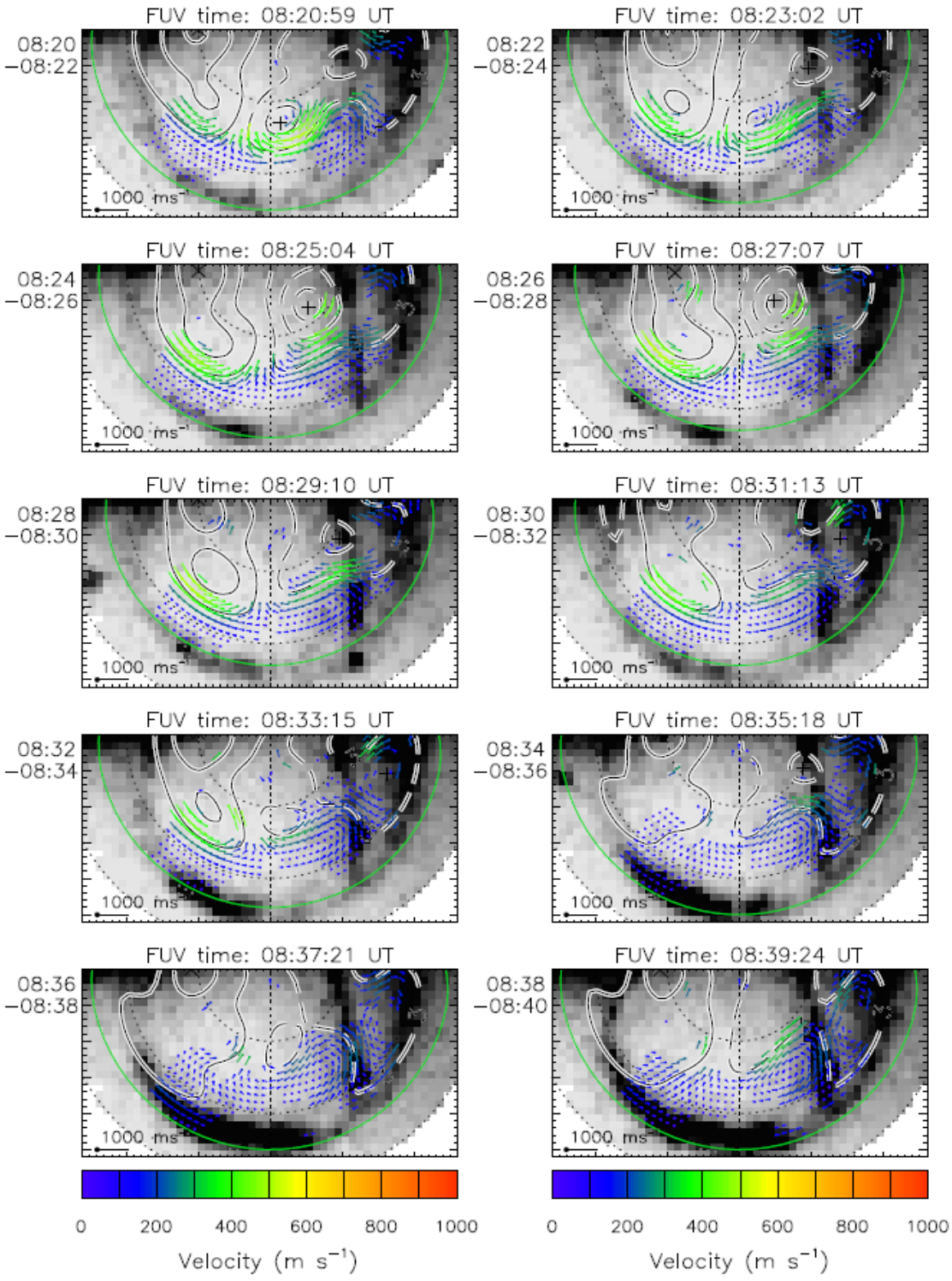

Figure S1(b). Continued.

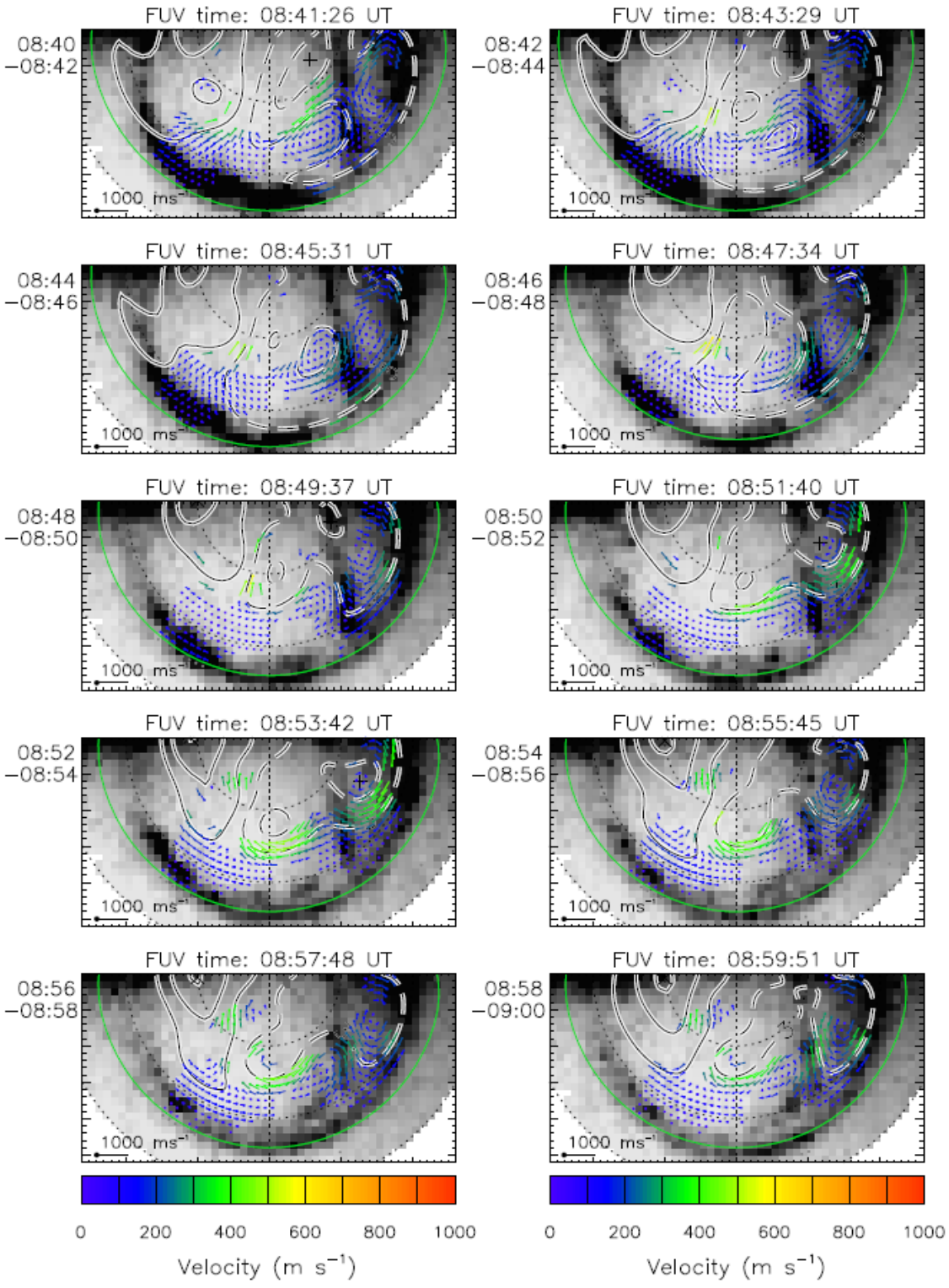

Figure S1(c). Continued.

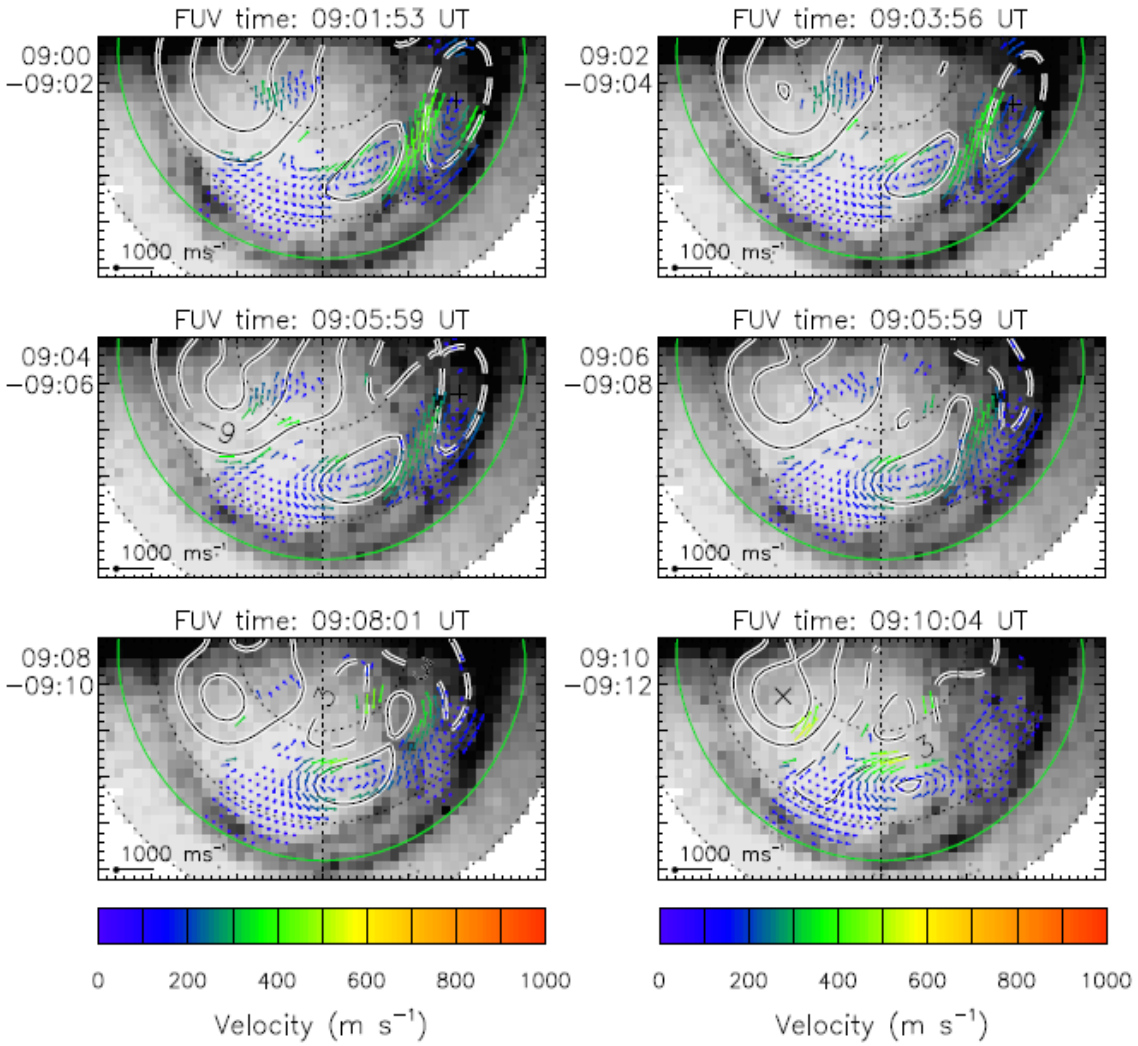

Figure S1(d). Continued.

Movie S1. The movie of the auroral imager data of the main theta aurora ovals and TPAs in the northern hemisphere in polar coordinates detected by the FUV-WIC onboard IMAGE, is displayed. Each image shown in the movie is projected onto magnetic latitude (MLat)-magnetic local time (MLT) coordinates. The top and bottom sides in each figure show the noon and nightsides whose MLT is 12h and 24h (0h), respectively. The dawn (6 MLTs) and dusk (18 MLTs) meridians correspond to the right and left sides, respectively. The color code is assigned according to the number of photons (the intensity of brightness) in units of Rayleigh. Possible dayglow contaminations were removed by setting IMAGE FUV-WIC data view software provided by the FUV-WIC team to the glow removal mode. Particular time annotations in the auroral imager snapshots at 7:27:48 UT, 8:14:51 UT and 9:10:04UT are inserted in order to notify the times of "TPA onset", "TPA brightening onset" and "TPA disappearance", respectively.

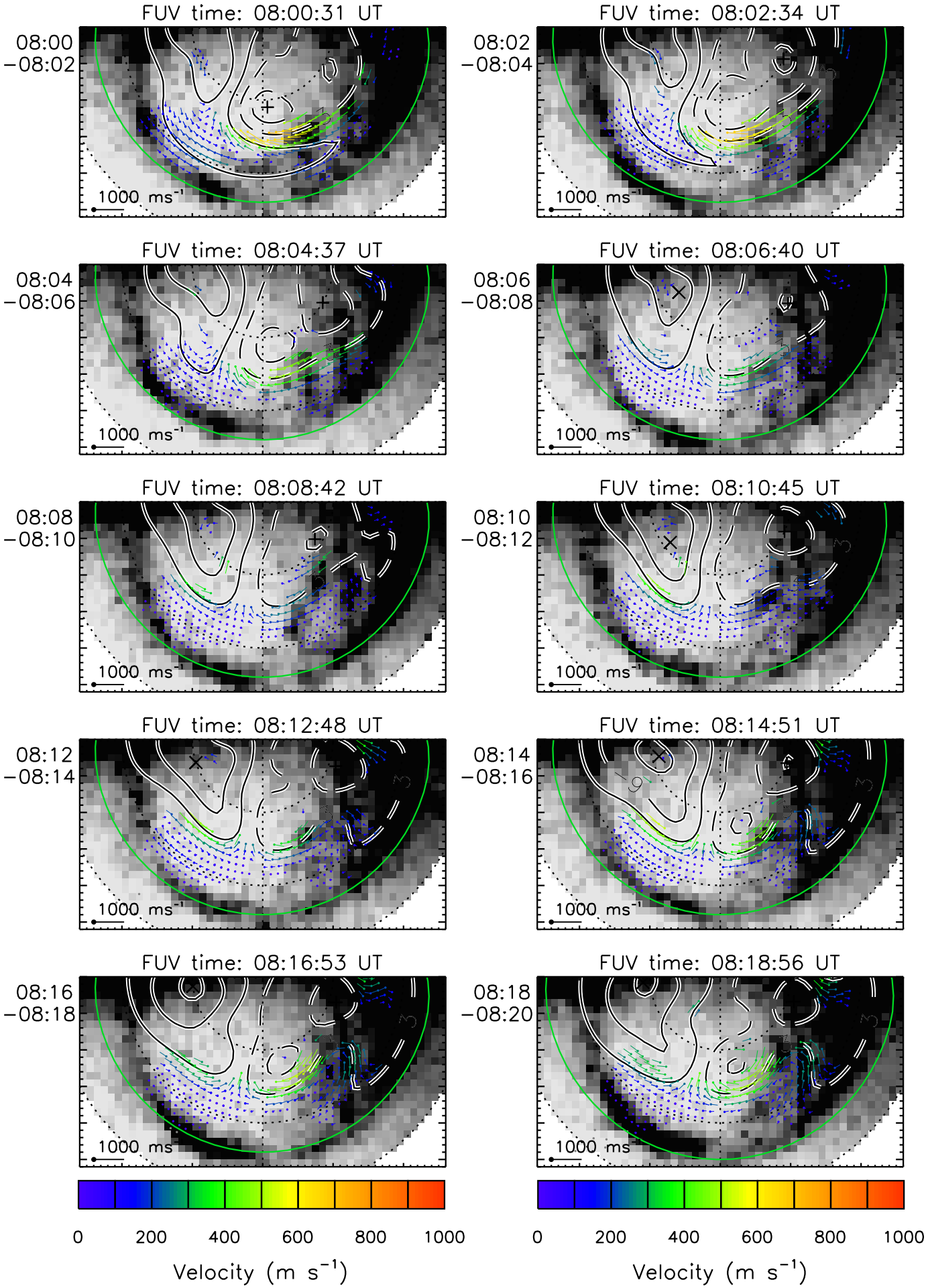
FUV time: 08:00:31 UT
08:00
−08:02
1000 ms⁻¹
FUV time: 08:02:34 UT
08:02
−08:04
1000 ms⁻¹
FUV time: 08:04:37 UT
08:04
−08:06
1000 ms⁻¹
FUV time: 08:06:40 UT
08:06
−08:08
1000 ms⁻¹
FUV time: 08:08:42 UT
08:08
−08:10
1000 ms⁻¹
FUV time: 08:10:45 UT
08:10
−08:12
1000 ms⁻¹
FUV time: 08:12:48 UT
08:12
−08:14
1000 ms⁻¹
FUV time: 08:14:51 UT
08:14
−08:16
1000 ms⁻¹
FUV time: 08:16:53 UT
08:16
−08:18
1000 ms
FUV time: 08:18:56 UT
08:18
−08:20
1000 ms
0
200
400
600
800
1000
Velocity (m s⁻¹)
0
200
400
600
800
1000
Velocity (m s⁻¹)

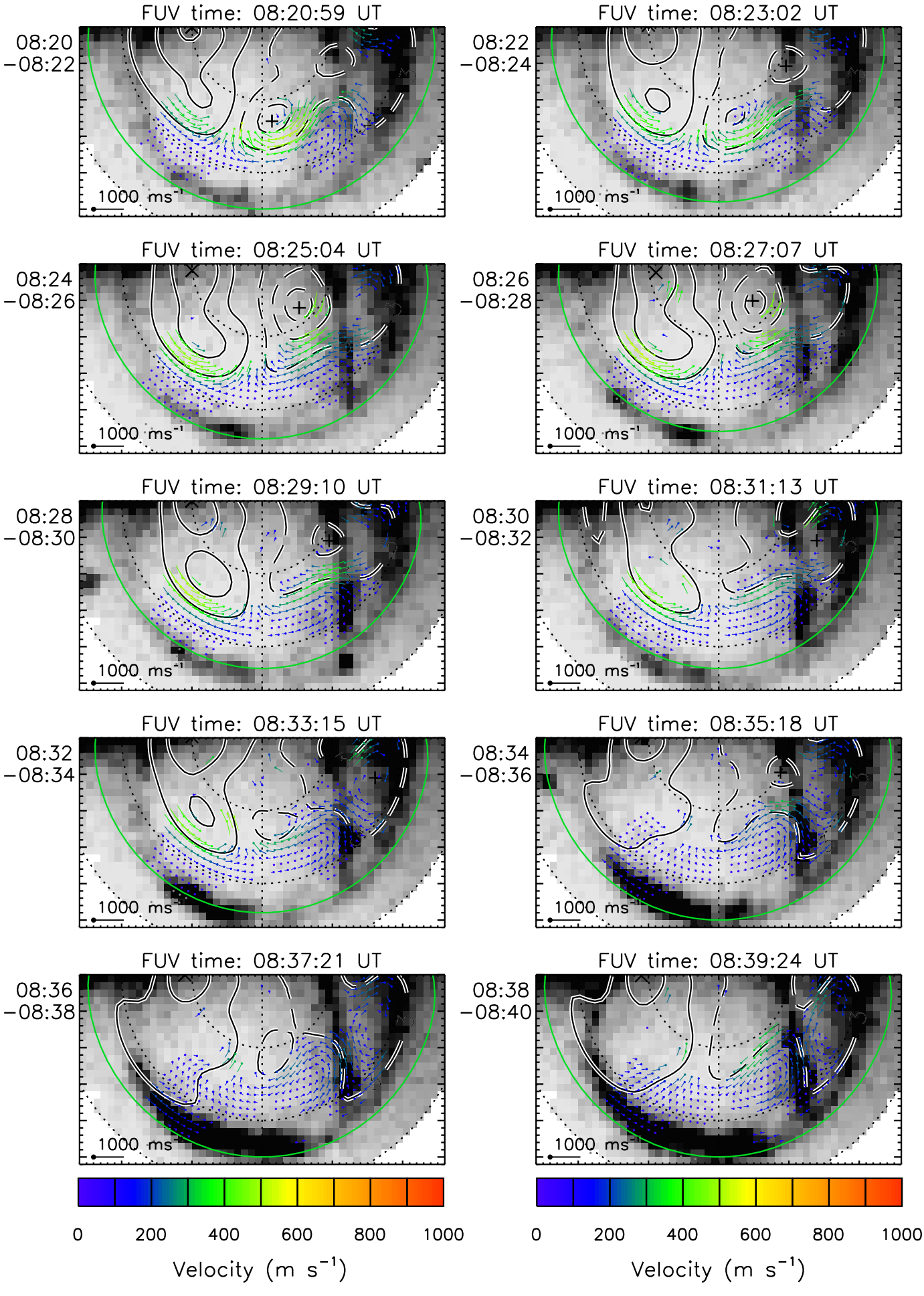
FUV time: 08:20:59 UT
08:20
−08:22
1000 ms⁻¹
FUV time: 08:23:02 UT
08:22
−08:24
1000 ms⁻¹
FUV time: 08:25:04 UT
08:24
−08:26
1000 ms⁻¹
FUV time: 08:27:07 UT
08:26
−08:28
1000 ms⁻¹
FUV time: 08:29:10 UT
08:28
−08:30
1000 ms⁻¹
FUV time: 08:31:13 UT
08:30
−08:32
1000 ms⁻¹
FUV time: 08:33:15 UT
08:32
−08:34
1000 ms⁻¹
FUV time: 08:35:18 UT
08:34
−08:36
1000 ms⁻¹
FUV time: 08:37:21 UT
08:36
−08:38
1000 ms⁻¹
FUV time: 08:39:24 UT
08:38
−08:40
1000 ms⁻¹
0
200
400
600
800
1000
Velocity (m s⁻¹)
0
200
400
600
800
1000
Velocity (m s⁻¹)

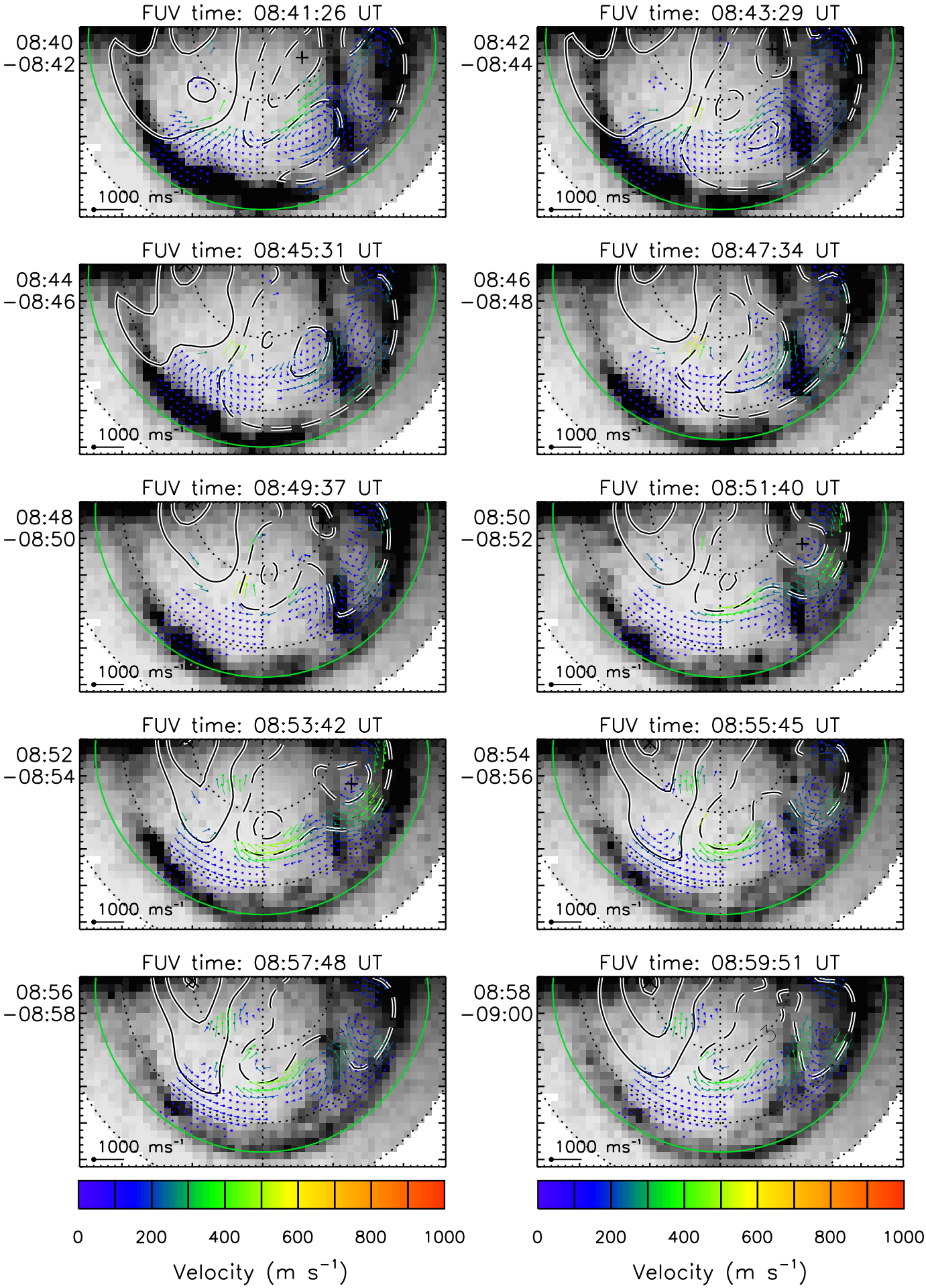
FUV time: 08:41:26 UT
08:40
−08:42
1000 ms⁻¹
FUV time: 08:43:29 UT
08:42
−08:44
1000 ms⁻¹
FUV time: 08:45:31 UT
08:44
−08:46
1000 ms⁻¹
FUV time: 08:47:34 UT
08:46
−08:48
1000 ms⁻¹
FUV time: 08:49:37 UT
08:48
−08:50
1000 ms⁻¹
FUV time: 08:51:40 UT
08:50
−08:52
1000 ms⁻¹
FUV time: 08:53:42 UT
08:52
−08:54
1000 ms⁻¹
FUV time: 08:55:45 UT
08:54
−08:56
1000 ms⁻¹
FUV time: 08:57:48 UT
08:56
−08:58
1000 ms⁻¹
FUV time: 08:59:51 UT
08:58
−09:00
1000 ms⁻¹
0
200
400
600
800
1000
Velocity (m s⁻¹)
0
200
400
600
800
1000
Velocity (m s⁻¹)

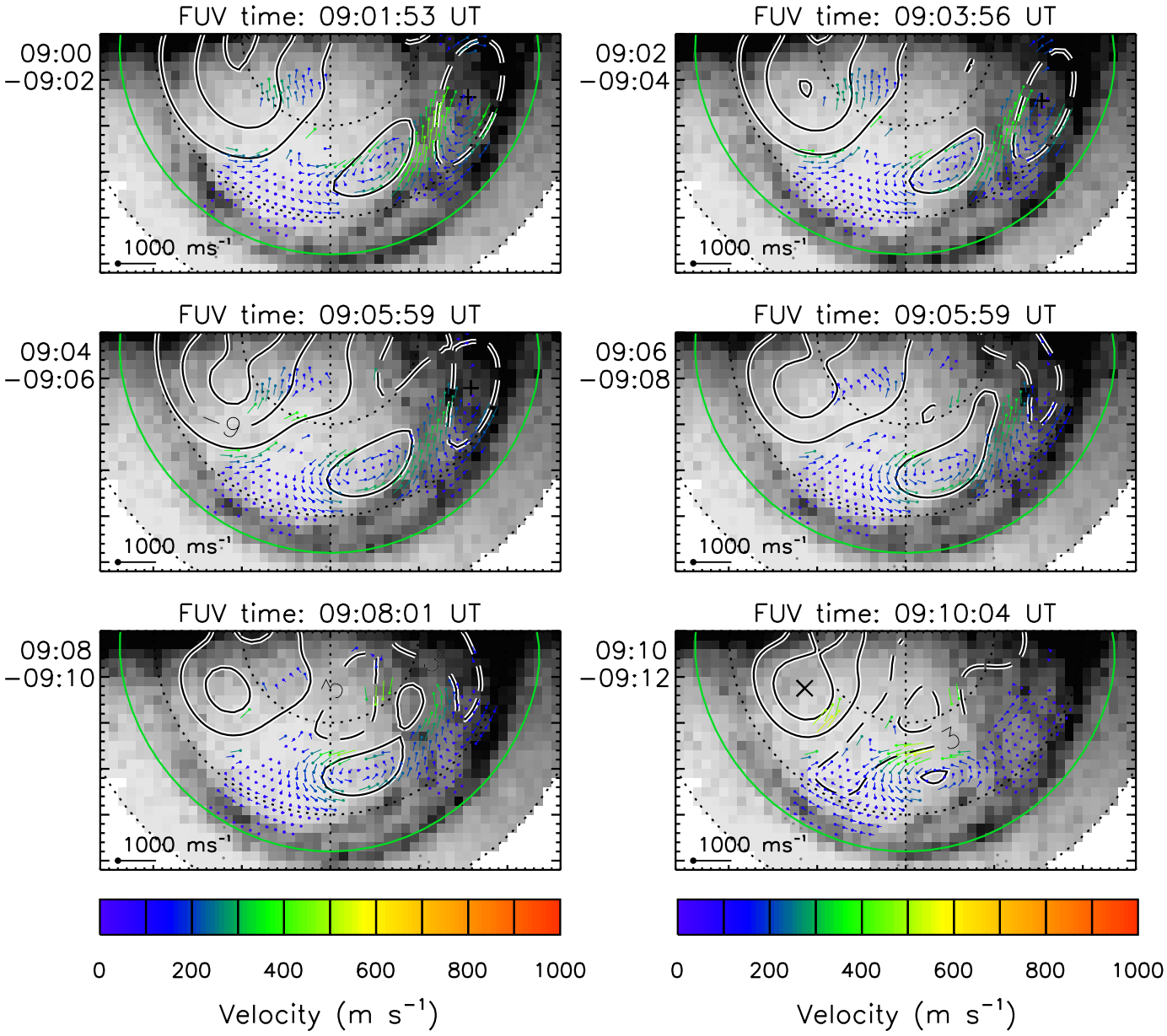
FUV time: 09:01:53 UT
09:00
−09:02
1000 ms⁻¹
FUV time: 09:03:56 UT
09:02
−09:04
1000 ms⁻¹
FUV time: 09:05:59 UT
09:04
−09:06
1000 ms⁻¹
FUV time: 09:05:59 UT
09:06
−09:08
1000 ms⁻¹
FUV time: 09:08:01 UT
09:08
−09:10
1000 ms⁻¹
FUV time: 09:10:04 UT
09:10
−09:12
1000 ms⁻¹
0
200
400
600
800
1000
Velocity (m s⁻¹)
0
200
400
600
800
1000
Velocity (m s⁻¹)